Princeton Plasma Physics Laboratory

PPPL- 4359

PPPL- 4359

Modeling of Carbon Migration During JET Injection Experiments

J.D. Strachan, J. Likonen, P. Coad, M. Rubel, A. Widdowson, M. Airila, P. Andrew, S.Brezinsek, G. Corrigan, H.G. Esser, S. Jachmich, A. Kallenbach, A. Kirschner, A. Kreter, G.F. Matthews, V.Philipps, R.A. Pitts, J. Spence, M. Stamp, S. Wiesen, and JET-EFDA contributors

October, 2008

PPPL
PRINCETON PLASMA PHYSICS LABORATORY

Prepared for the U.S. Department of Energy under Contract DE-AC02-76CH03073.

Princeton Plasma Physics Laboratory
Report Disclaimers

Full Legal Disclaimer

Trademark Disclaimer

PPPL Report Availability

Princeton Plasma Physics Laboratory:

http://www.pppl.gov/techreports.cfm

Office of Scientific and Technical Information (OSTI):

http://www.osti.gov/bridge

Related Links:

U.S. Department of Energy

Office of Scientific and Technical Information

Fusion Links

MODELLING OF CARBON MIGRATION DURING JET ^{13}C INJECTION EXPERIMENTS

J.D. Strachan[1], J. Likonen[2], P. Coad[3], M. Rubel[4], A. Widdowson[3], M. Airila[5], P. Andrew[3], S. Brezinsek[6], G. Corrigan[3], H.G. Esser[6], S. Jachmich[7], A. Kallenbach[8], A. Kirschner[6], A. Kreter[6], G.F. Matthews[3], V.Philipps[6], R.A. Pitts[9], J. Spence[3], M. Stamp[3], S. Wiesen[6], and JET-EFDA contributors[*].

JET-EFDA Culham Science Centre OX14 3DB, Abingdon, UK

[1] *PPPL Princeton University, Princeton, NJ 0854, USA*

[2] *VTT Technical Research Centre of Finland, Association EURATOM-Tekes, Finland*

[3] *UKAEA Fusion Association, Culham Science Centre, Abingdon, Oxon, UK*

[4] *Association EURATOM-VR, Royal Institute of Technology (KTH), Alfven laboratory, Stockholm, Sweden*

[5] *Helsinki University of Technology TKK, Association Euratom-Tekes, Finland*

[6] *Institut fuer Energieforschung-Plasmaphysik , Forschungszentrum Juelich, Association EURATOM-FZJ, Trilateral Euregio Cluster, D-52425, Juelich, Germany*

[7] *Ecole Royale Militaire, Brussels, Belgium*

[8] *Max-Planck-Institut fuer Plasmaphysik, EURATOM-Assoziation, Garching, Germany*

[9] *Ecole Polytechnique Federale de Lausanne (EPFL), Centre de Recherches en Physique des Plasmas, Association Euratom-Confederation Suisse, Ecole, Ch1015 Lausanne, Switzerland*

[*] See appendix of M.L. Watkins, *et al*, Fusion Energy 2006 (21st IAEA Int. Conf. Chengdu)

ABSTRACT

JET has performed two dedicated carbon migration experiments on the final run day of separate campaigns (2001 and 2004) using $^{13}CH_4$ methane injected into repeated discharges. The EDGE2D/NIMBUS code modelled the carbon migration in both experiments. This paper describes this modelling and identifies a number of important migration pathways: 1. deposition and erosion near the injection location, 2. migration through the main chamber SOL, 3. migration through the private flux region aided by **E**×**B** drifts, and 4. neutral migration originating near the strike points. In H-Mode, type I ELMs are calculated to influence the migration by enhancing erosion during the ELM peak and increasing the long-range migration immediately following the ELM. The erosion/re-deposition cycle along the outer target leads to a multistep migration of ^{13}C towards the separatrix which is called "walking". This walking created carbon neutrals at the outer strike point and led to ^{13}C deposition in the private flux region. Although several migration pathways have been identified, quantitative analyses are hindered by experimental uncertainty in divertor leakage, and the lack of measurements at locations such as gaps and shadowed regions.

1. INTRODUCTION

The interface of the core fusion plasma with the outside world occurs at plasma-facing components (PFC). These components present challenging materials issues for fusion reactors [1, 2]. The issues include the PFC erosion, migration and deposition at other vessel locations, its subsequent re-erosion, and re-deposition. Tritium retention in the PFC and co-deposited layers [3] is another important concern. This paper is aimed towards understanding the migration pathways including some aspects of the re-erosion processes. This paper's contribution is achieved by modelling ^{13}C migration during JET experiments in which $^{13}CH_4$ was injected [4].

Campaign integrated material migration has historically been difficult to analyze since the erosion and deposition measurements are only available through application of surface analysis on components removed after a campaign. Any results thus integrates over a range of plasma types (L-Mode, H-Mode, and advanced scenarios) as well as plasma geometries (different inner and outer strike point locations, and wetted areas) and divertor plasma parameters (temperatures, densities, heating power, radiation levels, and ELM types, frequencies, and amplitudes). Consequently, campaign integrated results are difficult to interpret quantitatively.

In contrast, ^{13}C injection experiments are ideal for modelling. Using the last run day of an experimental campaign, $^{13}CH_4$ is introduced repeatedly into a single plasma type so that the migration occurs under controlled conditions. A number of repeated discharges are used to ensure sufficient ^{13}C quantities for subsequent detection without perturbing individual plasmas [4]. Consequently, the modelling of the ^{13}C migration in such experiments is more constrained than the simulation of naturally sputtered carbon migration in campaign integrated experiments.

This paper reports EDG2D/NIMBUS based modelling of the ^{13}C transport in JET tracer injection experiments. Similar ^{13}C migration experiments have occurred on other devices such as TEXTOR [5, 6], DIII-D [7, 8], and ASDEX Upgrade [9]. These experiments have had their own emphasis and modelling efforts [10-12]. The present status of those studies has made inter-machine comparisons premature since each has had difficulty reaching an acceptable level of agreement between the modelling and experiment.

The principal outcome of the simulation effort described in this paper is the identification of the carbon migration pathways. These pathways include migration through the main chamber SOL, migration by a multi-step process involving erosion and local deposition (termed "walking" [13]), ion migration through the Private Flux Region (PFR), and neutral migration originating at the strike points and terminating at the PFR surfaces. The deposited fractions have several experimental uncertainties including leakage out of the gas injection module, and the multiple re-erosion steps. Not all of the injected ^{13}C has been found on representative PFC's removed from the divertor targets. The location of the remaining ^{13}C is projected to be on unmeasured surfaces such as the main chamber PFC as well as in gaps and shadowed regions in the divertor.

The outline of this paper is as follows. The injection experiment is described in Section 2. The deposition measurements are described in Section 3. The use of EDGE2D to model the migration is described in Section 4. The initial EDGE2D and ERO modelling of the ^{13}C migration are described in Section 5. Since this initial modelling agreed poorly with experiment, further effects had to be considered. In Section 6, effects of leakage from the gas injection system are described. This leads to introduction of ^{13}C into the main chamber. Since the subsequent migration of this leaked ^{13}C is governed by the same processes as for the 2001 top injected ^{13}C, comparison is made to those 2001 experiments. In Section 7, the effects of

erosion are described. The erosion causes a "walking" [13] migration along the outer target, which is described in Section 8. The walking leads to carbon neutral formation at the outer strike point and consequently neutral carbon migration to the PFR, which is described in Section 9. The total ^{13}C migration picture is discussed in Section 10 and compared to the campaign integrated JET carbon migration. The supporting evidence for each migration process is summarized along with limitations and possibilities for future work.

2. EXPERIMENT

The JET tracer injection experiments have been described previously [4, 14-17] and the relevant details are briefly repeated here. Two experiments were performed, one in 2001 and a second in 2004. The 2001 experiment injected methane at the top of the main chamber into a 2.4 T, 2.4 MA ohmic plasma. In 2004, the methane was injected about 5 cm above the outer strike point in the divertor into a 1.4 T, 1.4 MA H-mode plasma heated by 8 MW of deuterium neutral beams. The ELMs were type I with 120Hz frequency having an average core energy loss of about 30 kJ at each ELM. This paper is primarily concerned with modelling the 2004 experiment, although comparison is made to the 2001 experiment in Section 6.

Some details of the experiments require further description than previously reported:

1. The 2004 divertor tile geometry was shown schematically in figure 4 of [3] and is now shown with accurate relative dimensions in figure 1. The poloidal distance around the divertor is a distance that will be used to plot the deposition results and is measured along the red line in figure 1. That distance was also shown schematically in figure 4 of [3]. The actual geometry is important when identifying the shadows caused by tile structure on the straight line neutral carbon transport.
2. At the time of the 2004 experiment, a toroidally uniform gas injection module was assumed. However, the actual injector is composed of 48 separate injectors (figure 2), which are uniformly dispersed in the toroidal direction. The relative throughput of each injector is assumed identical. The injection occurs in the gap between Tiles 7 and 8 (see figure 1).
3. Leakage out of the gas injection pre-chamber to the top of tile 8 occurs. The leakage arises from a hole in the top of the pre-chamber which is in the range of 25% of the cross-sectional area of the slot between Tiles 7 and 8. This leakage allows methane to reach the main chamber outside of the divertor (on the top of the baffles). It may also have allowed ^{13}C to enter the PFR below Tile 7.
4. The density measured by the far-infrared interferometer in the edge regions (r/a = 0.9) were within 10% of the EDGE2D values. Also, divertor target Langmuir probe measurements were available during the 2004 experiment. The target electron density magnitude is consistent with the modelled values (figure 3) and the agreement is typical of that obtained by EDGE2D simulations. In EDGE2D, the ELMs modestly change the density values (see figure 3), so that ELM averaging of the density, as was done with the experimental data, should not change the agreement.The EDGE2D outer strike point (figure 3) seems to be displaced by nearly 1 mid-plane cm from the experimental data, with a smaller inner strike point effect. This displacement is common and is probably due to uncertainties in the EFIT reconstruction which provides the equilibrium used to generate the EDGE2D grid. Displacement of either strike point is unlikely to influence the modeling since erosion effects dominate this region. A further complication is that to obtain the divertor target profiles, the strike points were moved along the inner and outer targets for a 2 sec period during the beam heating on each discharge. There is legitimate concern that this movement influenced

migration along the targets, thus compromising the modelling which assumed stationary strike points.

3. DEPOSITION MEASUREMENTS:

The ^{13}C deposit measurement techniques have been described elsewhere [4, 14, 16, and 17] and in this section only the basic results will be summarized and updated with recent measurements including newly analyzed locations. The analyzed tiles were from two toroidal locations in the divertor.

The JET tiles exposed both in 1998-2001 and in 2001-2004 were analyzed by means of accelerator-based ion beam analysis (IBA) methods at the University of Sussex. The amount and distribution of ^{13}C were measured with nuclear reaction analysis (NRA) $^{13}C(^{3}He,p)^{15}N$ using a 2.5 MeV ^{3}He beam and with Rutherford backscattering spectrometry (RBS) using a 2.5 MeV H beam. Experimental RBS spectra were simulated with the SIMNRA program [16, 18].

Secondary ion mass spectrometry (SIMS) analysis [17] was made with a double focussing magnetic sector instrument (VG Ionex IX-70S) using a 5 keV O_2^+ primary ion beam to profile for the $^{12}C^+$ and $^{13}C^+$ secondary ions. A higher mass resolution of 2000 ($m/\Delta m$ at $m/q = 28$) was used to separate the element peaks from interfering isobars (e.g. $^{13}C^+$ from $^{12}CH^+$). The ^{13}C ion intensities were converted to total ^{13}C content by integrating through the surface layer, and comparing with the integrated result for two calibration samples that were measured separately with time-of-flight elastic recoil detection analysis (TOF-ERDA) [17].

Both the SIMS and IBA techniques result in deposit measurements with about 10% accuracy. The scatter of the data and the difference between the deposit measurements between the two techniques was usually less than 10% (figure 4). Regions with significant erosion (near the strike points) and thicker deposits of intrinsic carbon had larger than 10% point-to-point scatter. These are regions of larger surface roughness, which can make deposits more non-uniform [19]. Thus the surface roughness is expected to cause some of the scatter.

Since the first papers describing the 2004 injection experiment appeared, some new surface analysis results have become available. The most important of these, from the point of view of the simulations, are listed below:

1. A SIMS measurement was made from a shadowed region near the injector on Tile 7. In order to protect the edges of Tile 7, the divertor was designed so that magnetic field lines would leave a shadowed region on the front surface of the tile. This region had the largest ^{13}C deposit (see the location at 1600 mm in figure 4 and the discussion in Section 7). This is the only measurement in a gap or shadowed region reported here even though these are clearly important as final migration destinations.
2. IBA and SIMS measurements were made on Tile 5 at the floor of the divertor indicating that the centre of Tile 5 was a region of low deposition (figure 4) during the 2004 experiment.
3. SIMS measurements were made at a second toroidal location. This location was further from the leakage and the results indicate that the deposits were toroidally uniform except on Tile 8 (figure 4). The deposit on Tile 8 decreases consistent with $1/r^2$ where r is the distance from the measurement location to the point of the leakage. One interpretation is that the deposit found on the outer baffle top (Tile 8 at 1800 mm distance around the divertor) was due to gas expansion of the leakage methane. In that case, up to 50% of the injected methane would have entered the vessel through the leakage.
4. Shadows appear at 650 mm on Tile 4 and 1200 mm on Tile 6. Reductions in the deposits seem to be due to Tile 3 shadowing the inner strike point from Tile 4 and Tile

7 shadowing the outer strike point from Tile 6. Notice that the inner strike point must be a source of carbon neutrals comparable to the outer strike point. Large deposits exist on Tile 4 in the region of 600-700 mm distance around the divertor (figure 4) yet Tile 4 is shadowed from the gas injector as well as the outer strike point. These shadowing effects will be discussed further in Section 9.

5. The reciprocating probe at the top of the vessel was inserted during the 2004 experiment (figure 1 of [17]) with the deposition on a Silicon substrate being measured. During the experiment, the probe tip was 14 mm from the separatrix at its closest approach. The first depth profile measurement (at 4 mm from the probe tip) was thus located at 18 mm from the separatrix. It should be noted that although the distance to the separatrix is quoted to 1 mm precision, absolute uncertainties of that distance of about a cm do exist due to the same EFIT uncertainties which influenced the fit to the divertor Langmuir probe data (section 2.4). Here, the measurements of the ^{13}C deposits are extended to include SIMS depth profiling measurements (figure 5). The deposits are thicker on the side of the probe facing the flow of carbon ions from the outer to the inner divertor (the ion side). As the probe tip is approached, the ^{13}C deposits are less dense but extend deeper into the surface. The deposits were characterized by their depth as the distance into the surface where the ^{13}C density was ½ of the surface ^{13}C density. In figure 6, the ^{13}C depth is compared to surface roughness measurements of the probe performed after probe exposure. Notice that at the closest approach, the depth of the deposit increased even though the surface ^{13}C density decreased (see Section 7). The Si substrate surface was polished to better than 50 nm prior to the plasma exposure, and the surface roughness increased due to the plasma exposure. Part of the increase was due to Boron Nitride powder deposited from the probe housing and part was due to plasma bombardment. The roughness was greater than the deposit thickness on the electron side but less than the deposit thickness on the ion side. Both the deposit thickness and roughness increase for distances closer to the probe tip.
6. The SIMS depth profiles were also measured in the divertor regions (figure 7). The depth profiling along the outer target indicates high surface ^{13}C densities especially at the top of Tile 8 and low surface densities near the outer strike point. These ^{13}C densities are only a fraction of the surface deposits in these areas, and the composition of the total deposits are unknown. The deposit measurements along the inner target indicate deep ^{13}C deposits but with low surface density especially near the inner strike point. The deposits in the PFR and in the shadowed region of Tile 7 are characterized by flat profiles with steep spatial gradients on the interior. The deposit in the shadowed region is particularly thick. Parameterization of the depth profiles into the surface ^{13}C density and the depth of the deposit to ½ of that density were made. This characterization of the deposits indicates that the deposits are less dense at the strike points and are most dense at the top of Tile 8 and in the shadowed region of tile 7 (figure 8).

4. EDGE2D MODELLING

The goal of this section is to outline the computational strategy for modelling the migration, while the specific modelling results will be described more fully in the subsequent sections. A preliminary discussion of the modelling was reported in Ref. [20].

EDGE2D [21] is a 2D fluid edge code which models the plasma and impurity ions as separate fluids and the neutrals with a Monte Carlo code (NIMBUS). The fluid equations are applied for each cell in a grid where prominent sources of neutrals include gas puffing and

recycling locations. The neutrals are followed on straight trajectories beginning at a source or recombination and ending at ionization or wall impact. Upon ionization, then the fluid of each ionized species can move both parallel and perpendicular to the field lines. All ionization states of carbon are included. In the modeling, the carbon deposits are derived from carbon ion fluxes to the divertor targets and neutral carbon fluxes leaving the edge of the simulation grid. EDGE2D assumes that carbon is non-recycling so that it remains where it is deposited, and for this reason, post-processors were developed (Section 7) to consider further erosion of the deposited ^{13}C.

The cross-field transport is defined by transport coefficients either assumed or constrained by SOL measurements. The parameters used to fit the EDGE2D runs here were the density at the divertor targets measured by the Langmuir probes, the density at the plasma edge measured by the interferometer, the input power, and the energy drop at each ELM. The assumed parameters include the carbon particle diffusion coefficient, the thermal conductivities, and the sputtering coefficients. These assumptions are based upon previous EDGE2D studies where different features of the JET SOL were studied [*e.g.* 22-24]

Several EDGE2D studies have modeled methane injection on JET [22-24]. EDGE2D successfully described the screening of the injected methane [22] and the contamination resulting from intrinsic carbon sources, although the consequences of the leakage on core contamination will be reported in Ref [25]. The uncertainties associated with modelling methane injection by assumed atomic carbon injection have been described fully in [23]. A further issue is related to the grid itself which becomes coarse in the vicinity of Tile 8 just above the injector. This occurs due to the more grazing incidence of the field lines in this area, so the calculated deposits are not expected to be as accurate in this region. Another complication is that the Tile 8 geometry was changed slightly in the calculation from the actual experiment. This was necessary in order to accommodate the neutrals mesh. It is difficult to quantify the effect of these grid imperfections, but this is a region dominated by deposit from the leakage and there is little consequence to being unable to compare EDGE2D to experiment in this region.

In terms of carbon migration, one principal uncertainty is the carbon cross-field particle diffusivity, which is only weakly constrained by the core contamination that results from the methane injection. Figure 12 of [23] illustrates the results of a sensitivity analysis of the migration pathway of mid-plane injected carbon to several parameters including the carbon diffusivity. While the migration location indicates some sensitivity to the assumed carbon diffusion coefficient; the assumed electron and ion heat conductivities, the deuterium diffusion coefficient, and the density did not influence the final migration location. Variation of these parameters by a factor-of-two resulted in the 5% variations of the carbon fluxes to their final deposit locations (figure 12 of [23]).

In addition to the cross field carbon diffusivity, D_C, the EDGE2D calculated migration is sensitive to the ELM modelling, the main chamber SOL flow, and the $\underline{\mathbf{E}}\times\underline{\mathbf{B}}$ drift in the Private Flux Region. Since inclusion of each of these effects makes EDGE2D more unstable, they were included separately in different code runs. The approach used in this paper, has been to separate the calculations of the migration through the main chamber SOL from the those of the migration through the private Flux Region and so in this manner separate the effects of main chamber SOL flow from the $\underline{\mathbf{E}}\times\underline{\mathbf{B}}$ drift. This approach seems reasonable since the main chamber SOL flow does not influence the migration in the PFR, while the $\underline{\mathbf{E}}\times\underline{\mathbf{B}}$ drift is much less than the anomalous SOL flows in the main chamber. In contrast to the separation of the main chamber flow from the PFR drifts, the approach of separating the ELM effects is less valid but unavoidable, at present. The ELM treatment will be described shortly and is derived from the fact that the inter-ELM phase is responsible for most of the long-range migration. Since the inter-ELM phase is near the equilibrium SOL behaviour but at slightly

reduced input power, the steady-state EDGE2D solutions approximate the inter-ELM behaviour and thus can incorporate the **E**×**B** drifts or the main chamber SOL flow, depending upon whether the main chamber SOL or the PFR migration is being studied. During the ELM peak time, inertial effects dominate (due to the flow of particles from the main chamber SOL into the divertor), so that long-range migration is less likely. However, erosion is larger during the ELM peak and must be included in the re-erosion calculations which are performed in an EDGE2D post-processor.

The carbon migration in the main chamber SOL is influenced by the SOL flow in the main chamber. A parallel Mach number of about ½ with respect to the ion sound speed characterizes this flow, and classical calculations of the expected magnitude have been about 10 times lower than the experimental values [26]. Given the large discrepancy, the approach taken here is to induce a flow in the simulation by application of an external force [24]. The size of the force is adjusted until the SOL flow is matched to experiment. In this manner, the effect of the flow on the migration can be understood, even if its origin is not. The logic is that when the origin of the flow is understood, then the external force in the EDGE2D momentum balance will be replaced by an actual term of about the same value.

In the simulations described here, the ELM is described using the EDGE2D models developed in [27]. Its simulations matched experimental measurements from a well diagnosed JET plasma having ELMs with average ELM plasma stored energy drop of ~100 kJ. The energy and core density drop were achieved in EDGE2D by increasing the cross-field transport coefficients by a factor of 60 for the duration of the ELM (assumed to be 1 msec). The radial extent of the increase in the transport coefficients was determined by the post ELM temperature and density profiles in the plasma core and the radial extent of the target heating in the SOL. Unfortunately, for the tracer injection discharges discussed here, the experimental data is insufficient to constrain the simulations in the manner described in [27]. The same transport coefficient prescription as used in [27] has therefore been adopted here, with appropriate reductions in input power and deuterium gas puffing to match the lower power and density of the injection discharges. Likewise, the rise in transport coefficients during the ELM was reduced (to about a factor 20) to account for the lower ELM energy drop (~30 kJ) and the ELM duration shortened (to 0.1 ms) in accordance with experiment. Calculations with the same ELM energy loss achieved by primarily increasing the plasma diffusivity (simulating convective ELMs) or primarily increasing the electron or ion conductivity (simulating conductive ELMs) did not change the resulting carbon migration pattern.

The SOL energy flow components for the 30 kJ ELM are compiled in Figure 9. There are significant differences compared with the higher energy ELM used in [27]. In particular, the 100 kJ ELMs feature a cool phase immediately following the ELM where the SOL and divertor have little power influx, since most of the core power is rebuilding the pedestal. The 100 kJ ELMs in [27] can be pictured as a cycle in 3 phases: hot, cool and recovery phases; where the cool phase has the largest carbon long range migration. During the recovery phase, more long range migration can occur since conditions are favorable for such transport. In contrast, little migration is possible during the ELM peak (Section 5.1). The 30 kJ ELMs is approximated by a cycle of 2 phases: a hot phase and a recovery phase. This is evidently due to a reduced depletion of the pedestal by the smaller ELMs so that the migration results presented here are specific to the small Type I ELMs obtained during the tracer injection discharges and can be expected to differ qualitatively for larger ELMs.

5. INITIAL EDGE2D AND ERO RESULTS

This section presents initial migration results without the inclusion of erosion effects. In addition to the EDGE2D code simulations, initial modeling with the ERO [28] Monte

Carlo code has been performed and supports the EDGE2D conclusions. ERO is a 3D code which incorporates molecular break-up of the methane as well as re-erosion effects of the deposited ^{13}C. The background plasma has been taken from the EDGE2D runs. ERO was run in a manner similar to EDGE2D with methane molecular break-up being the only additional physics. In other words, the carbon was treated as a non-recycling material, and the results were toroidally averaged to examine the 2D behaviour. With these assumptions, ERO predicts ^{13}C deposition similar to that obtained by EDGE2D (figure 10), so that the initial migration of the methane injected can reasonably be approximated by atomic carbon injection as in EDGE2D.

Without ^{13}C recycling, most of the injected ^{13}C should be re-deposited back onto the injection region and both codes have poor agreement with experiment. Sections 6-9 describe refinements that have been applied to the simulations to produce the final overall fit presented in Figure 4. These refinements are often formulated in post-processor calculations using the EDGE2D background plasma and fluxes. Two aspects (ELM effects and **E**×**B** migration through the PFR) of the initial EDGE2D calculation are important and will be discussed further in Section 5.1 and 5.2.

5.1 ELM EFFECTS UPON MIGRATION

The ELM has two main effects on the carbon migration. Firstly, the ELM influences the parallel and perpendicular motion of the carbon by changing the parallel forces acting on it and enhancing the perpendicular carbon diffusivity in the ELM-affected region. Secondly, the ELM causes hotter plasma to interact with surfaces consequently increasing the re-erosion rate of the deposited carbon. The re-erosion effects will be treated in Section 7. In this section, the effects of the ELM on the carbon migration from the outer target to the inner target are examined.

During the ELM itself, power and particles flow into the main chamber SOL from the pedestal (figure 9). Consequently, the particle flow from the mid-plane to the divertor exerts a friction force on the carbon which prevents the injected ^{13}C from migrating far. However, in the inter-ELM time, the power from the core heats the pedestal region and less propagates into the SOL. During this time, the SOL and divertor plasmas are cooler, and the ^{13}C injected is ionized further into the divertor and some can escape the immediate vicinity of the target. The inter-ELM injected carbon can migrate further than that injected during the ELM.

The effect of the ELM can be most clearly seen on the migration to the inner target. The simulations indicate that the fractional ^{13}C deposits (y-axis of the figures) are much less during the ELM than inter-ELM. The deposit in the vicinity of the inner strike point (350 to 450 mm on Tile 2) is explained by the PFR migration (Section 5.2). The longer inter-ELM duration means that the total inter-ELM deposit is relatively larger when normalized to the total injected ^{13}C than shown in figure 11.

5.2 **E**x**B** DRIFT

Switching on **E**x**B** drifts in the PFR increases the simulated deposit in Figure 11 at the inner strike point. The gradients in the PFR are stronger than in SOL locations so that the radial electric field is correspondingly larger and the **E**x**B** drift is locally the largest in the entire plasma edge. The EDGE2D code calculates all the classical drifts but only the **E**x**B** drift acting close to the separatrix in the PFR is significant. This drift influences the carbon migration, but the actual flow pattern is complex (Figure 12). Carbon ions diffusing across the separatrix into the PFR feel this drift which drives the particles from outer to inner strike point (for the standard toroidal magnetic field direction of this JET experiment) and leads to

deposition near the inner strike point. Similar calculations but with the toroidal field direction (and hence the **E**x**B** drift direction) reversed reduce the simulated inner strike point deposition by about 3 orders of magnitude (Figure 11).

The EDGE2D calculations without re-erosion effects fortuitously fit the experimental deposition near the inner strike point (figure 11). EDGE2D indicates that the magnitude of the deposit at the inner strike point (350 to 450 mm on Tile 2 in figure 11) depends upon the magnitude of the carbon crossing the separatrix in the outer divertor leg. There is much evidence to indicate that erosion effects occur (Section 7), and erosion along the outer target increases the deposit near the inner strike point. Independent of the magnitude, the migration pathway for deposition in the vicinity of the inner strike point is through the PFR (figure 12).

By contrast, the deposition above the inner strike point (100 to 200 mm on Tile 1 in Figure 11) is form a migration pathway through the main chamber SOL. The inability of the EDGE2D calculation in figure 11 to describe the deposition on Tile 1 is an indication that more carbon escaped of out of the outer divertor into the main chamber SOL than was initially calculated by EDGE2D (Section 6).

6. LEAKAGE FROM THE GAS INJECTION SYSTEM

The escape of the injected ^{13}C into the main chamber SOL was probably not by the parallel ion transport or the escape of unionized neutral carbon out of the divertor. These effects were calculated in EDGE2D to be too small (Section 5, see figure 11). More likely, leakage at the baffle top of the injected gas (Section 2) allowed 15-50% of the injected methane to enter the main chamber, allowing ^{13}C atoms direct access the main chamber SOL. The experimental evidence for the leakage includes visible observation of the holes in the top of the pre-chamber at the injector, the high surface density of the ^{13}C deposits depth profiled at the top of Tile 8 (figure 7), and the toroidal non-uniformity of the deposits on Tile 8 (figure 4).

Figure 13 indicates EDGE2D calculations with carbon injection at the leakage location causing the observed deposits on the inner baffle. As before, the inter-ELM plasma is responsible for most of this long-range migration. The deposit on the inner baffle results from carbon which travels the length of the main chamber SOL. This deposit is in the range of 1-5% of the total injected ^{13}C indicating that about 5-50% of the injected carbon escaped the outer divertor into the main chamber SOL, but only a small fraction of that release travel all the way to the inner target. The physics describing this migration is the same as for the 2001 injection from the vessel top.

The 2001 JET experiment [3] injected $^{13}CH_4$ at one toroidal location at the machine top into a 2.4MA, 2.4T Ohmic plasma. Both the experiment [17] and the modelling [29] have been reported previously. The modeling of this first JET tracer experiment is also applicable to the leakage migration with the main difference being the actual location of injection in the main chamber SOL. In 2001, 50% of the ^{13}C was found and it was all deposited on the inner divertor target above the strike point [17] (figure 13). Computationally [29], three factors account for the deposition on the inner target. In order of importance:

1. Erosion rates are larger on the outer target so that deposits have more difficulty accumulating there [31].
2. The thermal force is larger near the outer (compared to the inner) divertor entrance causing the carbon to preferentially enter the inner divertor [29].
3. The experimental SOL flow is directed towards the inner target where it is measured at the machine top [31]. In the EDGE2D simulations of the 2001 experiment, a force was added to either/or both the deuterium and carbon in the main chamber SOL [24] of a magnitude so that the calculated flow matched the experimental measurement.

Computationally, the SOL carbon transport coefficients are only weakly constrained by experiment since the screening experiments [22] had a weak dependence upon the carbon SOL perpendicular transport. In order to explain the 2001 ^{13}C migration, EDGE2D simulations using different carbon cross field particle diffusivity, D_C, were tried until the inner target deposition was matched. For $D_C = 2$ m^2/s, about half of the carbon migrated to the inner target while the remainder was deposited on the main chamber walls (*i.e.* reached the edge of the main chamber grid). This magnitude would be consistent with both the inner target deposition and the methane screening experiments [22]. The deposition calculated in figure 13 does not have the peaks at 100 and 300 mm that were observed experimentally in 2001. Those experimental bumps could be reproduced if the EDGE2D SOL were assumed to have D_C radial variations of about factors of two. Alternatively the observed variations might be a consequence of the toroidally localized methane injection in 2001, so that the peaks were magnetic field line tied to the injection area while the valleys were not.

Such difficulties of interpretation indicate the limitation of a 2D code to explain the 2001 experiment and are one reason that the 2004 experiment was undertaken with toroidally distributed methane injection. It is notable that the inner target deposit obtained during the 2004 injection is smoother and does not possess the peaked structure found in 2001, even though the migration pathway is through the main chamber SOL in both cases. This observation either argues that the SOL D_C is different in H-Mode or that the toroidally localized injection in the 2001 ^{13}C experiment accounted for the spatial variations in deposition.

The EDGE2D calculation of the 2004 leakage migration is governed by the same physical phenomena as modelled in the 2001 experiment. In 2004, fewer ^{13}C were deposited on Tile 1 per injected ^{13}C since only a fraction escape through the leakage, and in 2004, the distance from the injection point to the inner divertor is longer allowing a higher chance of cross field diffusion to the wall. EDGE2D indicates that 10-45% of the leaked ^{13}C (or 5-25% of the injected ^{13}C) diffuses from the leakage location to the edge of the grid where EDGE2D assumes it is lost to the main chamber walls.

Experimentally, the 2004 deposits on the top of Tile 8 (outer baffle) were found to be toroidally inhomogeneous (figure 4), and were not measured at the leakage location. The calculation suffers since the injection location is near the grid edge where it connects to the junction of the outer baffle and the main chamber vessel. Possibly 5-30% of the total injected carbon (or 10-50% of the leakage ^{13}C) resides on unmeasured locations on the outer baffle. This fraction is so large since the throughput of the leakage might be large, as expressed by the model at 1600 to 1800 mm in figure 4. The combination of unmeasured locations on the main chamber walls and outer baffle, as well as unquantified leakage out of the gas injector limits the modelling ability to quantify this migration pathway. Moreover, since this pathway might involve 15-50% of the entire injected ^{13}C, the ability to model the total migration accurately is reduced.

The conclusion from this section is that the 2004 experimental inner target deposit on Tile 1 (above the inner strike point) originates from leakage at the top of the outer baffle causing carbon to be ionized directly in the main chamber SOL. Some carbon then travels along the magnetic field line the roughly 80 m distance to the inner divertor and enters the inner divertor leg much as main chamber injected carbon does, away from the separatrix due to the thermal force acting near both divertor entrances. Much of the carbon transports the roughly 5 cm mid-plane perpendicular (cross field) distances to be deposited on the main chamber walls. As discussed in Section 7, the carbon which travels along this path will also bring a ^{13}C flux onto the reciprocating probe which was inserted at the vessel top during the 2004 experiments. As a consequence, the deposit on that collector probe must be consistent with the inner target deposits above the inner strike point.

7. EROSION MODELLING

The EDGE2D calculations which agree with the measured inner target ^{13}C deposits on Tile 1 indicate a deposit on the RCP that is similar to the measured ion side deposit [17] for probe positions greater than about 5 cm from the separatrix (Figure 14). Near the probe tip (nearest the separatrix), the measured deposit was reduced in a manner consistent with erosion due to the hot plasma contact. Thus in order to simultaneously describe both the Tile 1 and the RCP deposits, erosion was assumed to occur near the probe tip. A model for the erosion along the RCP is developed in this Section and is applied to the outer target in Section 8.

A simple calculation of the residual ^{13}C deposit in the presence of significant erosion can be derived from a ^{13}C particle balance into the surface. The rate of change of the residual carbon surface density $^{13}\Omega$ (measured in particles / cm^2) is the difference between the fluxes into and out of the surface

$$d/dt\ ^{13}\Omega = \Gamma_{in} - \Gamma_{out} \qquad (1)$$

The flux into or out of the surface, Γ, is measured in particles / cm^2 / sec, and

$$\Gamma_{in} = f\ ^{13}R \qquad (2)$$

where ^{13}R (in units of particles/s) is the total ^{13}C injection rate and f is the fraction of ^{13}R (per cm^2) which reaches the surface. The EDGE2D simulations calculate f for each location assuming no re-erosion. In the absence of erosion, the deposit surface density increases with the injection duration according to:

$$^{13}\Omega = f\ ^{13}R\ \Delta t \qquad (3)$$

where Δt = 1.5 s is the exposure time of the RCP (several reciprocations into the injection discharges of 155s total injection duration). The y-axes in figures 4 and 14 are the values of $^{13}\Omega / (^{13}R\Delta t)$, or, equivalently, the factor f computed by EDGE2D.

The flux of ^{13}C out of the surface is determined by the deuterium sputtering of a pure ^{12}C surface reduced by the ratio $^{13}C/^{12}C$.

$$\Gamma_{out} = Y\ \Gamma_D\ ^{13}\Omega/^{12}\Omega \qquad (4)$$

where Γ_D is the EDGE2D computed flux of deuterium to the surface and Y is the carbon sputtered yield. Y is normally calculated in EDGE2D on the basis of published physical and chemical sputtering yields. Here, however, Y has been fixed to a given percentage (see figure 14 for the effect of the different levels) to allow the sputtering of freshly deposited material to be different than for a carbon substrate. The best fit was obtained with 5% sputtering yield which is about an order of magnitude higher than the expected physical sputtering.

Thus in steady-state ($\Gamma_{in} = \Gamma_{out}$), so:

$$^{13}\Omega/^{13}R = f\ ^{12}\Omega\ /\ Y\ \Gamma_D \qquad (5a).$$

Or in the units of the y-axis of figures 4 and 10:

$$^{13}\Omega/\ ^{13}R\ \Delta t = f\ ^{12}\Omega\ /\ Y\ \Gamma_D\ \Delta t \quad (5b).$$

Equation (5) indicates that the residual deposit on an eroding surface depends upon the ratio of the fraction of the ^{13}C which migrates to that surface and the eroded flux due to sputtering from that surface. Thus in the application of equation (5) to the RCP deposits, the reduced deposit at the probe tip is a consequence of the sputtered flux becoming larger than the depositing flux closer to the probe tip (figure 15). Equation (5) can be expressed in general as a steady-state residue of the deposition being a function of the two fluxes and the sputtering yield (figure 16) and is also applied to the outer target (Section 8).

The erosion model for the residue described by equation (5) follows from the depth profile observations (figure 5 and 8). The depth profiling found that regions of high erosion process had increased surface roughness. The deposit depth was comparable to the surface roughness. Therefore the sputtering ions can access the entire deposit depth. The consequence is that the ^{13}C residue probability of being sputtered is in proportion to its fraction of the total surface density. Thus instead of an erosion model which assumes a preliminary stage with a build up of material in regions of high erosion [32], this paper assumes that the erosion mixes the deposits into the substrate.

8. MIGRATION OR WALKING ALONG THE OUTER TARGET

The residue calculation that applied to the RCP in Section 7 also describes the residue on other surfaces and is used in this section for the outer target in the region between the injector and the outer strike point (figures 4 and 10). Without erosion effects, EDGE2D predicts a deposit about 2 orders of magnitude greater than measured, with the exception of a shadowed region on the tiles, which will be discussed shortly (figure 10). Use of equation (5) in post-processing the EDGE2D fluxes indicates that 5-10% sputtering yields can account for the residue. High sputtering yields might be expected since TEXTOR measurements indicate that chemical re-erosion of freshly deposited carbon atoms can be an order of magnitude higher than for bare graphite surfaces [33]. In fact, the range of phenomena that occur on amorphous carbon films re-deposited in fusion devices is complex, even when surface roughness issues are not considered [34]. Although a precise description of the sputtering is beyond EDGE2D, the simple residue formula from Section 7 did allow agreement with the deposit profile shape and magnitude. This agreement indicates that high re-erosion has occurred. The residue pattern is consistent with 5-10% sputtering by the calculated deuterium fluxes along the outer target.

The consequence for the carbon migration modeling is important since without re-erosion, carbon is expected to reside along the outer target and the actual deposit is 20-50 times lower (figure 10). Both the injected and eroded ^{13}C have low probability of escaping the outer divertor area into either the main chamber SOL or the PFR. For the PFR, the walking mechanism for the escape of carbon is proposed here (figure 17 illustrates a 3 step migration). The carbon releases from the target or injector as a neutral and thus is emitted isotropically. The carbon is subsequently ionized within a cm from the release location. EDGE2D indicates that the friction force (due to the flow of the deuterium particles from the main chamber and even more so during an ELM peak) dominates the carbon flow and forces the carbon back to the target. The ions must follow the field lines, and so re-deposit a step closer to the outer strike point than they started (figure 17). The walking process is entirely due to the angle between the field lines and the target and for the JET geometry results in a walking towards the separatrix. A similar mechanism was considered in [35] for the movement of tritium towards the inner louvres on JET. In fact, this process exists in re-erosion codes [e.g. 35, 36,

and 37] and even in EDGE2D if recycling was used for carbon. The 2004 JET ^{13}C experiment can be thought of as a clear example which emphasizes this mechanism.

The walking causes the eroded ^{13}C to sequentially deposit and re-erode nearer the separatrix until it crosses into the PFR and escapes the erosion/deposition cycle. The carbon undergoes 5-10 such re-erosion steps in the particular JET experiment described here taking about 10-50 msec to reach the separatrix. EDGE2D does not follow the re-erosion, but simulations varying the location of the carbon injection (figure 18), indicate that about 1/2 of the C eroded within 1 cm of the outer strike point enters the PFR as neutrals during the inter-ELM period. Figure 18 indicates that 40-60% of the ^{13}C that actually entered the gap between Tiles 7 and 8, reaches the PFR as neutrals and 5-20% as ions. The remainder is either deposited in gaps or on Tile 7 near the outer strike point.

5-15% is lost to gaps and shadowed regions during the stepwise migration along the outer target. The amount lost into the tile gaps is assumed proportional to the relative surface area of the tile gaps for each step and is therefore not accurately calculated. TEXTOR experiments indicate the importance of gaps and shadowed regions [38-40], but the deposition in the JET gaps has been measured only at the shadowed region on the front face of Tile 7 (figure 17 insert). The measured ^{13}C deposit on the Tile 7 shadowed region was similar (factor of 3 smaller) to the EDGE2D calculation without erosion, indicating that the lack of ion erosion in these areas accounts for the relatively large deposits. Thus the re-deposits in this area were not subject to walking since they were not re-eroded. Likely the deposition in the shadowed-region must be from neutrals since the magnetic field lines (which intersect this region) end on Tile 8. In EDGE2D, the deposit is due to ions impacting regions where the field lines or grid did not intersect Tile 8 and thus EDGE2D should not provide a good simulation of the shadowed areas. ERO will eventually provide a better simulation of the deposits in this area.

The multi-step erosion process at the outer target causes 10% of the injected carbon to enter into the PFR as ions. This is about 100 times more C ions entering the PFR than calculated in Section 5.2 (figure 11). These ions deposit primarily at either the inner or outer strike points. Thus an increased deposit occurs in the vicinity of the inner strike point (figure 19) over that presented in Section 5.2. Subsequently, those deposits are further eroded. The processes are complicated and here the assumption was made to use the residue calculation with an inter-ELM depositing flux and an ELM peak eroding flux (figure 19) to describe the deposits near the inner strike point. The inner strike point is only a temporary stopping spot for the ^{13}C with it ultimately being formed into a neutral and migrating to the PFR. The actual conversion process was not modelled and plausibly occurs during the ELM peak due to the higher temperatures and sputtering fluxes along the inner target at those times.

In summary, this section has considered the walking of the injected ^{13}C along the outer strike point. This walking moves the ^{13}C to the separatrix, so that the deposits near both strike points are erosion residue similar to those described along the RCP in Section 7.

9. NEUTRAL MIGRATION

One consequence of the stepwise migration is the resultant neutral carbon migration into the PFR originating from both the inner and outer strike points. Neutral migration occurred in the experiment as indicated by the shadows of the divertor tiles seen in the PFR deposits (Section 3.4). The magnitude of this neutral deposit is proposed to be a consequence of the walking along the outer target. Although difficult to simulate, the ELMs are envisioned to play a major role in this process. The ^{13}C deposits at or just below both the inner and outer strike points are due to ion deposits and are influenced by the ELMs. The increased power fluxes during ELMs must lead to enhanced erosion in these regions. The erosion will cause

further neutral loss. Ion emission from the surface will be re-deposited in the same region and be subject to erosion by the next ELM. Ultimately, the ^{13}C deposits measured on plasma-facing surfaces are the result of a dynamic balance between deposition and re-erosion while the majority of the carbon undergoes neutral transport to reside in gaps and shadowed regions or in the PFR.

About 10% of the injected ^{13}C was observed as deposits on exposed regions of the PFR (integral of the deposition pattern in figure 20). The magnitude is less than might be expected from the post-processed EDGE2D calculations. The PFR deposits experience further erosion due to D neutrals. TEXTOR [38] also documented erosion due to D neutrals. In the JET case, the neutrals must originate at the core or the strike points. The interesting aspect of this neutral erosion is that the top of Tile 5 has been subject to preferential neutral erosion compared to the deposits on Tile 4 and 6. This result may be due to a higher (or more energetic) flux of neutral deuterium bombarding Tile 5. Apparently, the deuterium neutrals reflected from the strike point regions must leave with a distribution around the complementary angle between the separatrix and the tile at the strike point (see figure 17, arrow at strike point). This angle would cause higher neutral deuterium fluxes to Tile 5, but is different than the cosine distribution about the normal angle which is commonly assumed for recycled neutral emission [*e.g.* 41].

The EDGE2D post processor calculated this neutral erosion using the inter-ELM deuterium neutral flux from the outer strike point, and the ELM peak value from the inner strike point with each emitted with a Cos^2 distribution. These fluxes were used with equation (5) to calculate the residue on Tiles 4, 5, and 6 (figure 20). Thus by assuming a 5% sputtering yield (with eqn. 5), the EDGE2D fluxes reasonably predict the PFR deposition pattern. Spectroscopic measurements also indicate that hydrocarbon layers may be formed on Tile 5 which can be more effectively eroded than graphite [42] and thus explain the high value of the sputtering yield used.

Neutral migration into the PFR has been used previously to explain the DIII-D ^{13}C deposition H-Mode experiments [43, 44]. The idea proposed here is slightly different, in that the neutral migration in DIII-D was attributed to the fact that the plasma was detached at both the inner and outer divertor legs (except during the ELMs). Under such conditions, the DIII-D neutral carbon is created by recombination in the detached region and can then transport as neutrals to locations with sightlines to the detached layer. For the neutral migration reported here, the outer target is attached and the inner at most only partially detached (see Figure 3) so that the migration occurs under attached plasma conditions.

10. DISCUSSION

In figure 21, the 2001 and 2004 ^{13}C experimental results are compared to campaign integrated migration results. The campaign integrated JET deposition of ^{12}C inside the divertor [45, 46] has been measured on W marker tiles [4] indicating that the outer target region is a region of erosion, the PFR is a region of high deposition, and some deposition also occurred at the top of the inner target. Using the modeling of the ^{13}C deposition pattern to interpret the ^{12}C campaign integrated deposits suggests the campaign integrated C deposits feature similar patterns as were observed in the ^{13}C deposits. Specifically:

1. The deposit on the top of the inner target (Tile 1) is likely due to carbon arriving at the divertor from the main chamber SOL (possibly sputtered from the main chamber walls).

2. Less ^{12}C was seen on Tile 4 compared to ^{13}C but more was seen on Tile 6. Both PFR deposits are likely the result of neutral transport originating from the inner and outer strike points and the Tile 6 deposits might indicate that sputtering from the outer strike point

during higher power and larger ELMs might be more important than during these ^{13}C injection experiments.

The JET ^{13}C experiments have proven valuable in forcing the subsequent modeling to include a variety of transport and plasma-surface interaction phenomena and thus to identify the important migration processes. The status of the modelling might be summarized as follows:

1. Modeling and measurement of the deposits at the inner and outer targets unambiguously identify leakage of a significant fraction of the outer divertor injected ^{13}C through the outer baffle and into the main chamber. Leakage occurred at the gas injection system.
2. The ^{13}C migrating to the inner target through the main SOL deposits preferentially above the inner strike point. By providing a satisfactory match to the measured profile, the EDGE2D simulations indicate that the weaker thermal force at the inner divertor entrance than at the outer (due to the different parallel temperature profiles) is an important factor. The main SOL flow also contributes but the relative importance of these two effects is untested by the ^{13}C injection experiments. Future tracer experiments in reverse field would almost certainly reveal the relative importance of these two processes.
3. The modelling indicates that inter-ELM periods are more favourable for long-range migration than the ELM peak times. However, the ELM peak is more important for erosion. The fact that the ^{13}C injection was time independent while the carbon sputtering evolves through the ELM cycle indicates that ^{13}C migration studies do not reproduce the plasma encountered sputtered carbon. Further experiments varying the ELM size or embedding ^{13}C in the divertor might help the modelling more accurately simulate the migration of sputtered carbon.
4. Erosion is required to explain the low observed deposits near the inner and outer strike points and at the reciprocating probe tip. Depth profiling measurements indicate that erosion did take place. An erosion model was developed based upon increased surface roughness being observed at the erosion locations. The model was developed to describe the RCP erosion, and later used to describe the divertor erosion. A description should be attempted which models the actual surface and the interactions with the sputtering ions..
5. A multi-step recycling model called walking was proposed to explain the absence of ^{13}C at the outer target. These vertical target shots are similar to the ITER targets. Experiments that change the angle between the field lines and the target surface would test this aspect of the modelling. Identification of the walking process during detachment along the target would also improve the utility of the models.
6. The **E**×**B** drift seems to adequately explain the migration of ^{13}C ions through the PFR to the inner strike point where it is subsequently eroded ending as deposits in the PFR. This pathway is unambiguous since deposits occurred in regions shadowed from the outer target. The **E**×**B** drift was required in order to deposit ^{13}C at the inner strike point where it could be eroded once more. However, the details of this pathway are untested due to its complexity (figure 12). Reverse field experiments might aid in quantifying the processes by reversing the **E**×**B** drift in the PFR.
7. Erosion at both the inner and outer strike points created C neutrals there which migrate along straight lines causing the PFR deposits. The observation of shadows in the deposit makes this pathway unambiguous. However, since the ELMs complicate both the neutral formation and walking migration along the outer target, the modelling was not strongly tested. Moreover, in ITER, the PFR is likely to have

short neutral mean free path in contrast to these JET experiments, so future experiments at higher PFR neutral density might elucidate the neutral migration.

8. The smaller deposit on the middle divertor base plate (Tile 5) than nearby (Tiles 4 or 6) is speculated to arise from further erosion due to neutral deuterium fluxes originating at the strike points. The role of ELMs and the angular and energy distribution of these fluxes are uncertain. The literature indicates that such neutral deuterium erosion can occur, but is not strongly tested by the modeling presented here.

11. CONCLUSIONS

The 2004 H-Mode JET ^{13}C methane injection experiments and simulations, described here, have revealed several migration pathways. With considerable uncertainty, a possible picture of the carbon migration was developed and is shown in Figure 22. ^{13}C deposits along the inner target on the SOL side of the inner strike point arrives at the inner divertor leg from the main chamber SOL. Carbon at the inner strike point arrives via PFR ion transport aided by the **E**x**B** drift in the PFR. The deposits at the inner strike point remain after re-erosion where ELM effects may be important. Deposits on the PFR side of the inner strike point arrive by neutral C transport across the divertor originating near the outer strike point. Deposits in the PFR are due to neutral transport originating at the outer or inner strike points and have a shadowed structure due to geometrical effects indicating long neutral mean-free-paths in the PFR for these experiments. These deposits also are subject to further erosion from deuterium neutrals that originates at the outer and inner strike points. The deposits on the outer target are mainly the residual from re-erosion along the outer target. A multi-step migration called walking seems to occur along the outer target allowing carbon to cross into the PFR.

Acknowledgment: This work, supported by the European Communities, was carried out within the framework of the European Fusion Development Agreement. The views and opinions expressed herein do not necessarily reflect those of the European Commission. JDS was supported by US DOE.

References:
[1] A. Loarte, *et al*, Nuclear Fusion **47**, S203 (2007)
[2] G. Federici, *et al*, Nuclear Fusion **41**, 1967 (2001), ITER generic Site Safety report GSSR III [G 84 RI 3 01-07-13 R1.0] p.4
[3] R.A. Pitts, *et al*, Plasma Physics and Controlled Fusion Research **47**, B303 (2005)
[4] J.P. Coad, *et al*, Nuclear Fusion **46**, 350 (2006)
[5] M. Rubel, *et al*, Vacuum **70**, 423 (2003)
[6] P. Wienhold, *et al*, J. Nuclear Materials **290-293**, 362 (2001)
[7] S.L. Allen, *et al*, J. Nuclear Materials, **337-339**, 30, (2005)
[8] W. Wampler, *et al*, J. Nuclear Materials **337-339**, 134 (2005)
[9] E. Vainonen-Ahlgren, *et al*, J. Nuclear Materials **337-339**, 55 (2005)
[10] A. Kirschner, *et al*, J. Nucl. Mater. **290-293**, 238 (2001)
[11] A.G. McLean, *et al*, J. Nuclear Materials **337-339**, 124 (2005)
[12] J.D. Elder, *et al*, J. Nuclear Materials **337-339**, 79 (2005)
[13] word suggested by J.D. Elder, 2007
[14] M. Rubel, *et al*, Vacuum **78**, 225 (2005)
[15] J.P. Coad, *et al*, J. Nucl. Mater. **363-365**, 287 (2007)
[16] M.J. Rubel, *et al*, J. Nuclear Materials **329-333**, 795 (2004)
[17] J. Likonen, *et al*, Fusion Engineering and Design **66-68**, 219 (2003)
[18] Mayer M. 1997 SIMNRA User's Guide, Report IPP 9/113 (Max-Planck-Institut für Plasmaphysik, Garching, Germany)
[19] D. Hildebrandt, *et al*, Physica Scripta **T81**, 25 (1999)
[20] J.D. Strachan, *et al*, 2007 Proc. 33rd ES Conf on Controlled Fusion and Plasma Physics (Warsaw, Poland) Vol. **31F** P1.030
[21] R. Simonini, *et al*, Contrib. Plasma Phys. **34**, 364 (1994)
[22] J.D. Strachan, *et al*, Nuclear Fusion **43**, 922 (2003)
[23] J.D. Strachan, *et al*, Nuclear Fusion **44**, 772 (2004)
[24] J.D. Strachan, *et al*, J. Nuclear Materials **337-339**, 25 (2005)
[25] J.D. Strachan, *et al*, 2008 PSI Conference – in preparation
[26] S.K. Erents, *et al*, Plasma Phys. Control. Fus. **42**, 905 (2000)
[27] A. Kallenbach, *et al*, PPCF **46**, 431 (2004)
[28] A. Kirschner, *et al*, Nuclear Fusion **40**, 989 (2000)
[29] J.D. Strachan, *et al*, 2004 Proc 30th EPS Conf on Controlled Fusion and Plasma Physics (London UK) Vol 28G (ECA) P-1.136
[30] K. Ohya, Jap. J. Appl. Phys. **42**, 5769 (2003)
[31] R.A. Pitts, *et al*, J. Nucl. Mater. **337-339**, 146 (2005)
[32] A. Kallenbach, *et al*, J. Nucl. Mater. **363-365**, 60 (2007)
[33] A. Kirschner, *et al*, J. Nucl. Mater. **328**, 62 (2004)
[34] G. Federici and C.H.Wu, J. Nuclear Materials **207**, 62 (1993)
[35] A. Kirschner, *et al*, Plasma Physics Contr. Fusion **45**, 309 (2003)
[36] K. Ohya, *et al*, J. Nucl. Mater. **363-365**, 78 (2007)
[37] J. Brooks, Fus. Eng. Des. **60**, 515 (2002)
[38] P.Wienhold, *et al*, Physica Scripta **T94**, 141 (2001)
[39] M. Rubel, *et al*, Physica Scripta **T111**, 112 (2004)
[40] A. Litnovsky, *et al*, J. Nuclear Materials **337-339**, 917 (2005)
[41] W. Eckstein and H. Verbeek, Nuclear Fusion: Data Compendium for Plasma Surface Interactions, Special Issue 1984, 12 (1984)
[42] S. Brezinsek, *et al*, J. Nucl. Materials **337-339**, 1058 (2005)
[43] W.R. Wampler, *et al*, J. Nuclear Materials **363-365**, 72 (2007)
[44] J.D. Elder, *et al*, J. Nuclear Materials **363-365**, 140 (2007)

[45] A. Kirschner, *et al*, IAEA 2006 paper EX/3-5
[46] J. Likonen, *et al*, J. Nucl. Mater. **363-365**, 190 (2007)
Figure Captions:

Figure 1 JET divertor poloidal cross section during the 2004 ^{13}C methane injection experiment is shown. The solid arrow indicates the methane injection location while the hollow arrow indicates the location of the leakage. The line along the tile surfaces indicates the path of the poloidal distance, which along with the tile numbers are used in subsequent figures.

Figure 2 Plasma facing side of Tiles 7 and 8 (figure 1) on the outer divertor, indicating the gas injection locations, the outer strike point, and some measurement locations (see Section 3)

Figure 3 The divertor Langmuir probe measurements of the electron density on both the inner (top) and outer (bottom) target. The lines indicate the EDGE2D values for the same locations at both the ELM peak and the inter-ELM times. The x-axis is the mid-plane position of the Ψ value at the probe and the range of values was obtained by sweeping the plasma past the probe. The negative numbers are in the PFR. The top x-axis is the poloidal distance around the divertor which will be used in subsequent plots for the ^{13}C deposits. The top axis is obtained for the stationary equilibrium, and this plot is essentially assuming that the target densities are unchanged by the sweeping. The measured outer target values peaks away from the separatrix. The difference of about 1 mid-plane cm or 3.5 target cm originates uncertainties in the EFIT reconstruction.

Figure 4 The deposited ^{13}C normalized to the amount injected for the 2004 experiments is plotted against the poloidal distance around the divertor (see figure 1). The solid line is the final result of the modeling.

Figure 5 The SIMS depth profiles of the ^{13}C deposits for locations on the ion side (top) and electron side (bottom) of the RCP. The ion side faces the field lines connected to the outer target and has thicker and deeper deposits. The distances indicate the distance of the measured depth profile from the probe tip which was inserted closest to the separatrix.

Figure 6 The thickness of the ^{13}C deposits and the surface roughness of the RCP are plotted against the distance from the probe tip. The distance of 0 is the end of the probe, which was closest to the separatrix (about 14 mm). The average surface roughness was measured after plasma exposure. Prior to plasma exposure, the Si substrate was polished to < 50 nm.

Figure 7 Log-log plots of the SIMS depth profiles of the ^{13}C deposits on the surfaces of the divertor with the arrows indicating the location of each depth profile. The y-axis for each depth profile ranges from 10^{20} to 10^{22} /cm^3 covering 2 orders of magnitude in ^{13}C deposit density. Below 10^{20} ^{13}C / cm^3, the natural ^{13}C isotope in the carbon substrate becomes important. The x-axis is the depth ranging from 10 to 10^4 nm covering 3 orders of magnitude. The depth profiles in figure 5 on the RCP could be shown to lower densities since the substrate there was Si. Although the axes are difficult to see in this figure, the important feature is the overall shape indicating regions of deposit and regions of erosion.

Figure 8 The surface thickness and surface density of the ^{13}C deposits in the divertor for the 2004 experiment plotted against the poloidal distance around the divertor. The surface density is the ^{13}C density at the front surface of the Tile.

Figure 9 Power balance from the EDGE2D modeled ELM indicates that during the 0.1 msec ELM the power across the separatrix peaks at 30 MW and the power to the target peaks at 10 MW. The power lost to the walls (or grid edge in the calculation) is negligible and the power lost as carbon radiation only equals the power to the target in the inter-ELM duration. The core energy lost in these ELMs was about 30 kJ, compare to the larger ELMs of [27] which lost 100 kJ/ELM.

Figure 10 The top graph expands the outer target region showing also the final fit (solid curve) (figure 4).The bottom graph shows the deposition in the 2004 experiment plotted *vs.* the poloidal distance around the entire divertor with the initial EDGE2D (long dashed line) and ERO (short dashed line) modeling results.

Figure 11 The ^{13}C deposition on the inner target plotted against the poloidal distance around the divertor. The lines indicate EDGE2D calculated deposition patterns due to the ELM peak (long-short dashed line), the inter-ELM time with either forward (solid line) or reverse **E**×**B** drifts (short dashed line). The forward **E**×**B** drift in the inter-ELM time accounts for the deposition near the inner strike point.

Figure 12 The carbon velocity vectors averaged over all the charge states for the EDGE2D calculation with carbon injected in the outer divertor, and the intra-ELM plasma (solid line in figure 11). Notice that the vectors point from outer target to inner target in the Private Flux Region near the X-Point. These vectors are reversed if the fields are reversed so that the **E**x**B** direction is reversed. The maximum velocity is about 8 km/sec corresponding to a vector about 5 cm long on the spatial scale of the 2D plot.

Figure 13 The deposition on the inner target for the 2004 experiment (squares) and the 2001 experiment (circles). The model for the 2001 experiment is the solid line [29]. The dashed line is 15% leakage the 2004 experiment modeled similarly to the 2001 experiment but with a different source and grid. The dashed dot line is the solid line in figure 11. Notice that the inner strike point was different between 2001 and 2004.

Figure 14 The 2004 SIMS (circle) and IBA (squares) measurements of the ^{13}C deposition on the RCP. The solid line with square markers is the EDGE2D based calculation of the deposit with no erosion and 15% leakage (the dashed line in figure 13). The remaining curves indicate possible effects of erosion where the carbon sputtering coefficient is a variable.

Figure 15 The EDGE2D calculated ^{13}C deposition flux and the carbon sputtering flux plotted as a function of the RCP location. The sputtering yield was assumed to be 5% in order to estimate the carbon sputtering flux from the EDGE2D calculated deuterium flux.

Figure 16 The steady-state ^{13}C residual deposit on a surface, which is subject to deposition and erosion by deuterium at a percentage sputtering yield indicated on the curves. The y-axis has the units of figure 4, and thus required a duration to be specified which was taken as 1 sec in this figure.

Figure 17 This schematic diagram indicates the carbon walking along the outer target. The location of the shadowed region is shown in the insert. The trajectory of carbon neutrals eroded off the outer target is assumed isotropic, while the trajectory of carbon ions is along the filed lines. The ions are forced back to the target by the inertia force. The neutral escape

into the PFR is assumed isotropic for carbon and with a $\cos^2$ distribution around the reflection angle for deuterium.

Figure 18 The one-step fractional escape of carbon ions and neutrals from the SOL into the PFR as a function of the puffing location along the outer target. Two sets of EDGE2D calculations are used, one for the ELM peak and another for the inter-ELM period.

Figure 19 The deposition is plotted along the inner target. The short dashed line was the solid line from figure 11 which is the initial EDGE2D calculations of the ion flux exiting the outer separatrix and travelling through the PFR to the inner strike point. The long-dashed line enhances this flux due to walking along the outer target and includes a neutral deposit at > 400 mm which originated at the outer strike point. The solid line indicates the final fit and includes not only the leakage flux (poloidal distance up to 300 mm) from figure 13, and also the reductions of the long dashed line due to erosion by ions at the ELM peak (300 to 440 mm) and inter-ELM D neutrals (>400 mm).

Figure 20 The ^{13}C deposition is plotted in the private flux region using the data and symbols from figure 4. The long dashed line indicates the neutral deposition originating at the outer strike point and enhanced by walking. The short dashed line indicates additionally the neutral deposition from the inner strike point. The solid line is the final fit and includes additionally the effect of neutral erosion by D neutrals originating from both strike points.

Figure 21 The deposition from both of the ^{13}C experiments overlaid with the campaign integrated deposition of ^{12}C (diamonds). The circles are the deposits from the ^{13}C injected at the vessel top (2001), while the squares are the deposits from ^{13}C injected near the outer strike point (2004). While the total injected ^{13}C in figure 4 is known, the total campaign integrated sputtered carbon here is not well known. In this figure the total sputtered carbon was assumed to be the sum of all the divertor deposits. This idea might be justified since the main chamber is a net carbon erosion zone.

Figure 22 EDGE2D calculated carbon plasma ion density summed over all ionization states when all the carbon originates by injection at the solid red arrow. The green arrows indicate the migration pathways described in this paper.

Figure 1

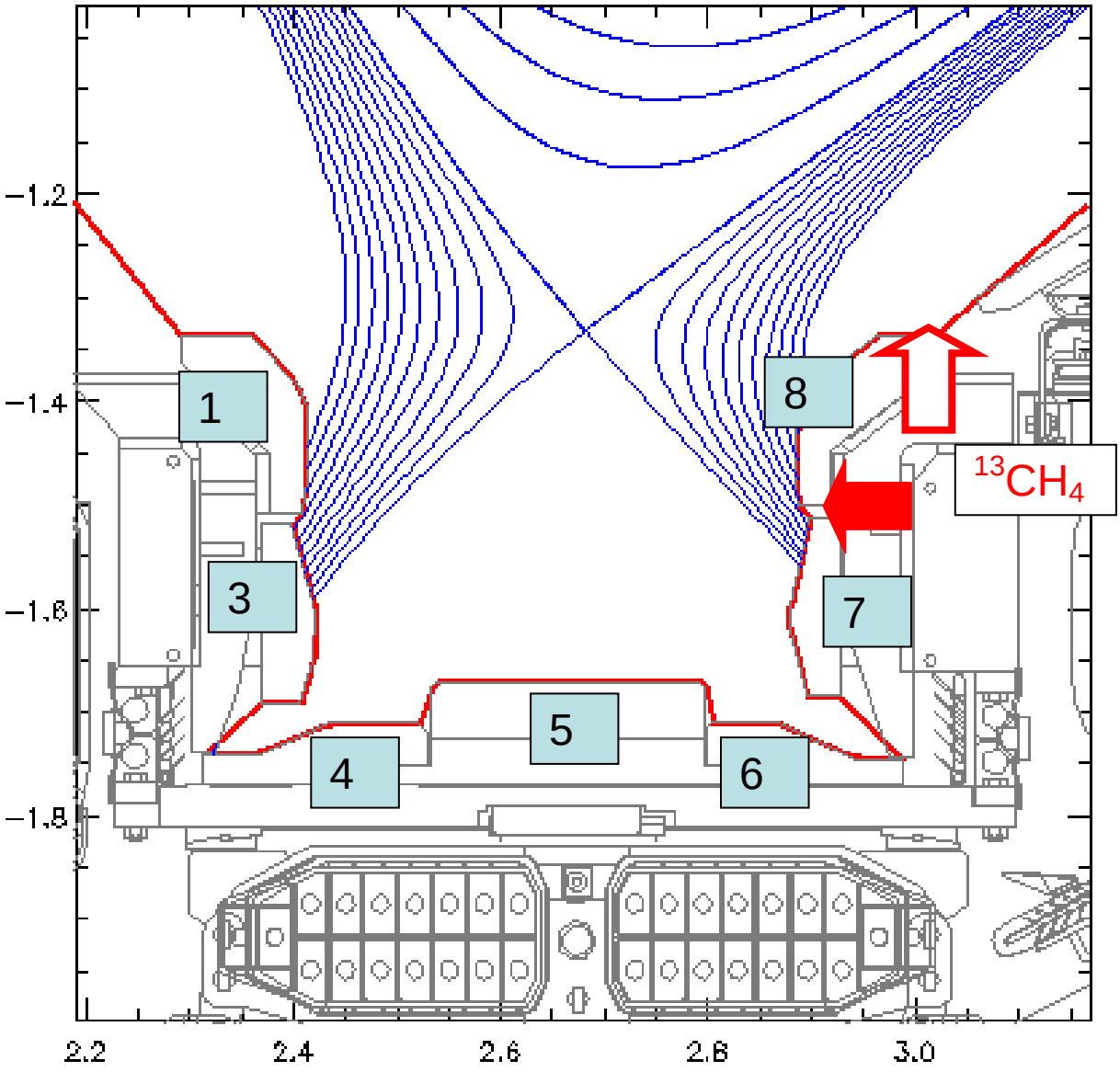

Figure 2

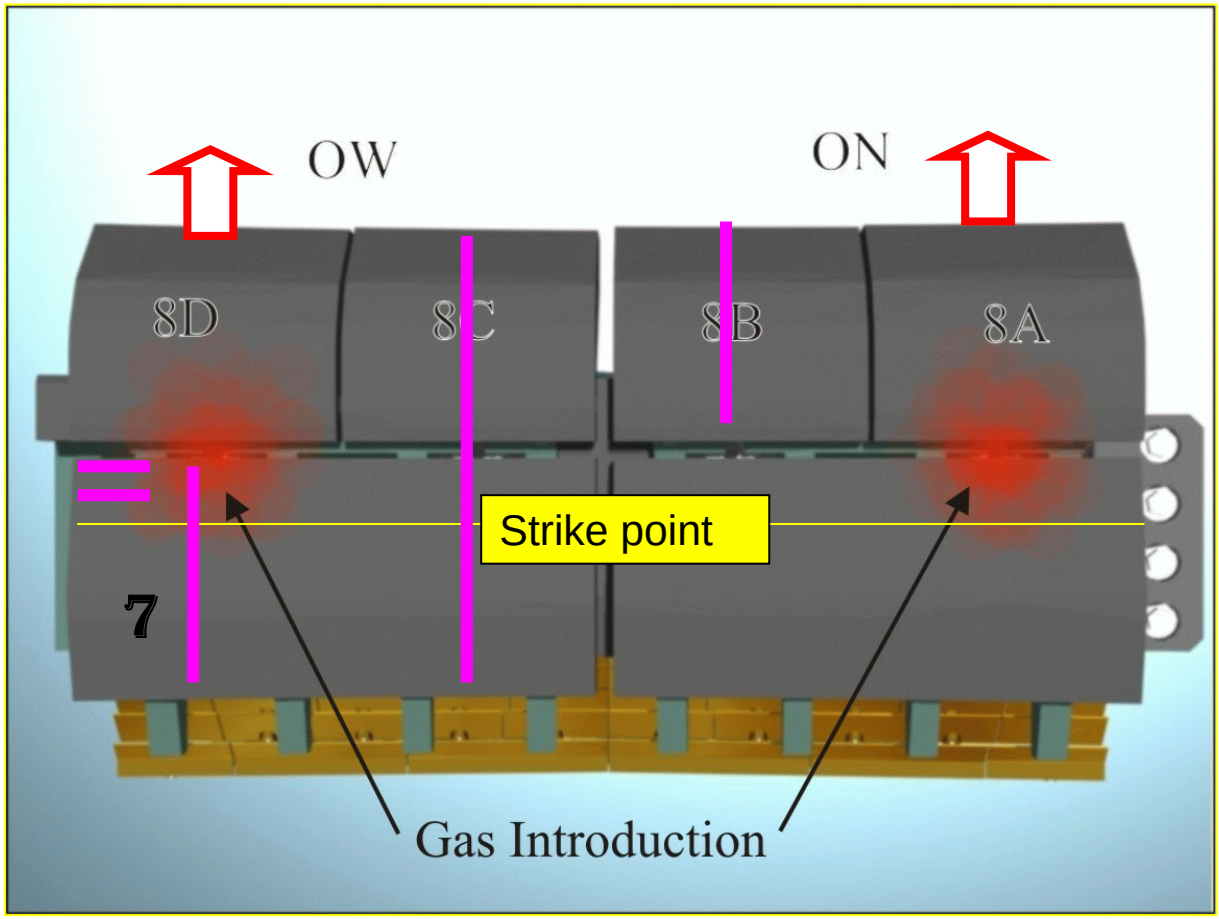

Figure 3

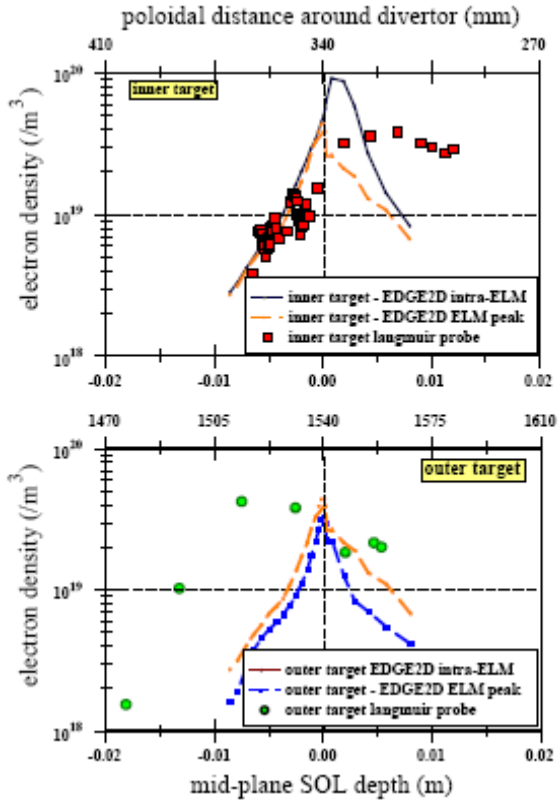
poloidal distance around divertor (mm)
410
340
270
inner target
electron density (/m^3)
10^{20}
10^{19}
10^{18}
inner target - EDGE2D intra-ELM
inner target - EDGE2D ELM peak
inner target langmuir probe
-0.02
-0.01
0.00
0.01
0.02
1470
1505
1540
1575
1610
outer target
outer target EDGE2D intra-ELM
outer target - EDGE2D ELM peak
outer target langmuir probe
mid-plane SOL depth (m)

Figure 4

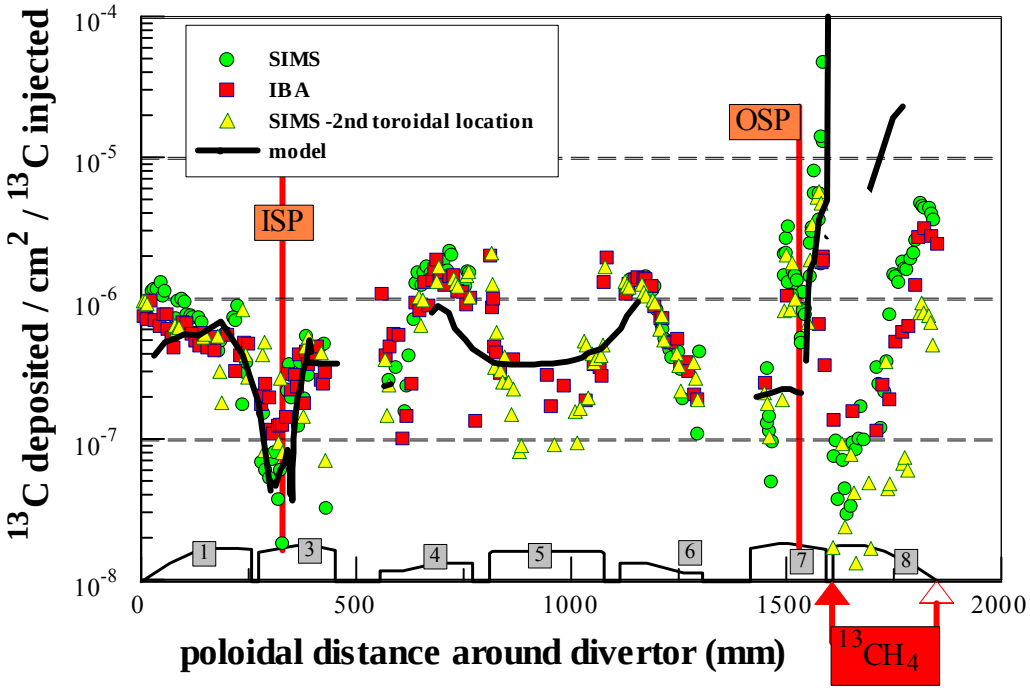
SIMS
IBA
SIMS -2nd toroidal location
model
ISP
OSP
^{13}C deposited / cm^2 / ^{13}C injected
poloidal distance around divertor (mm)
$^{13}CH_4$
1
3
4
5
6
7
8

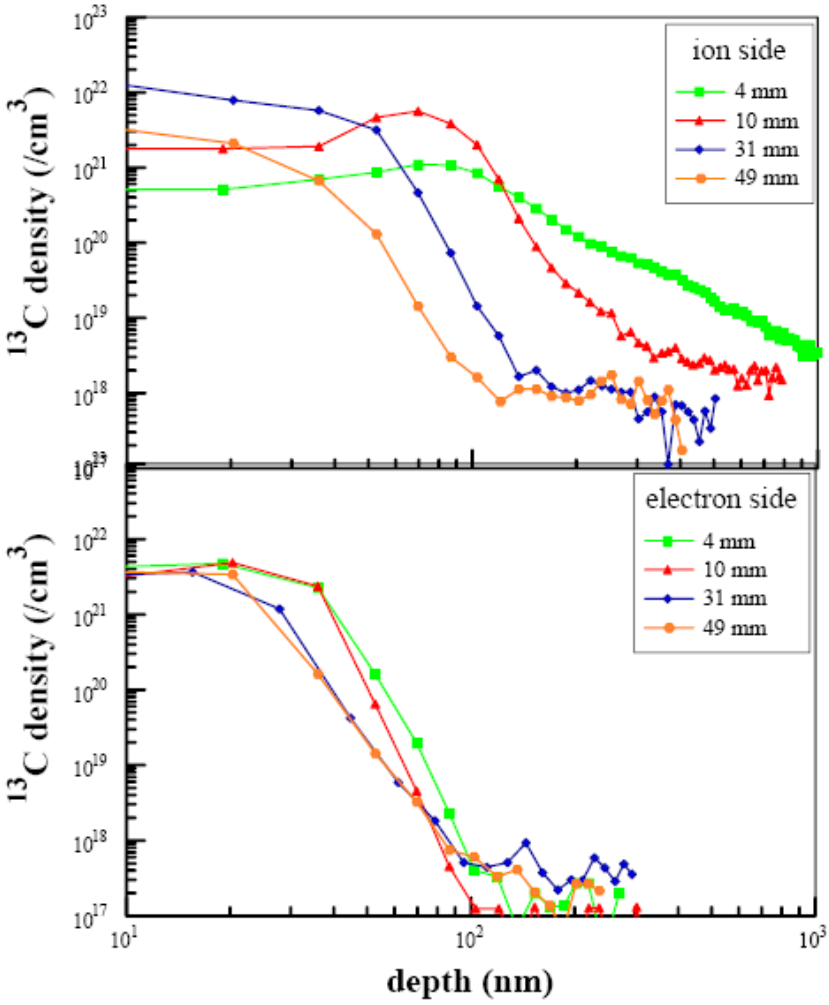
ion side
4 mm
10 mm
31 mm
49 mm
electron side
4 mm
10 mm
31 mm
49 mm
^{13}C density (/cm^3)
^{13}C density (/cm^3)
depth (nm)

Figure 5

Figure 6

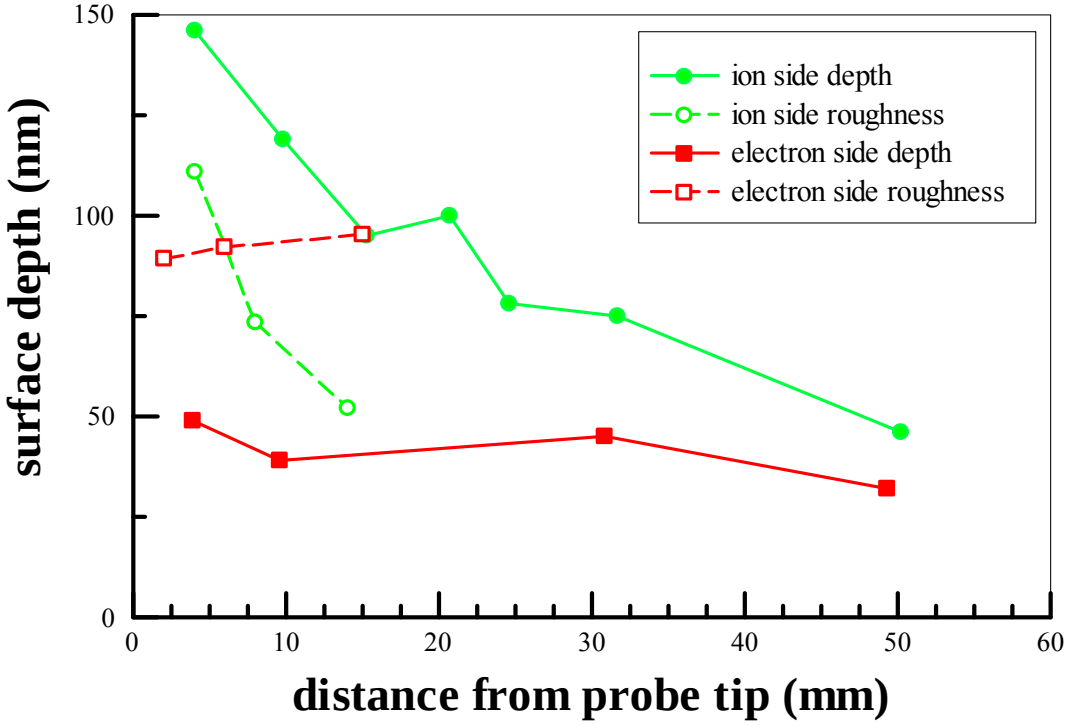
150
100
50
0
surface depth (nm)
0
10
20
30
40
50
60
distance from probe tip (mm)
ion side depth
ion side roughness
electron side depth
electron side roughness

Figure 7

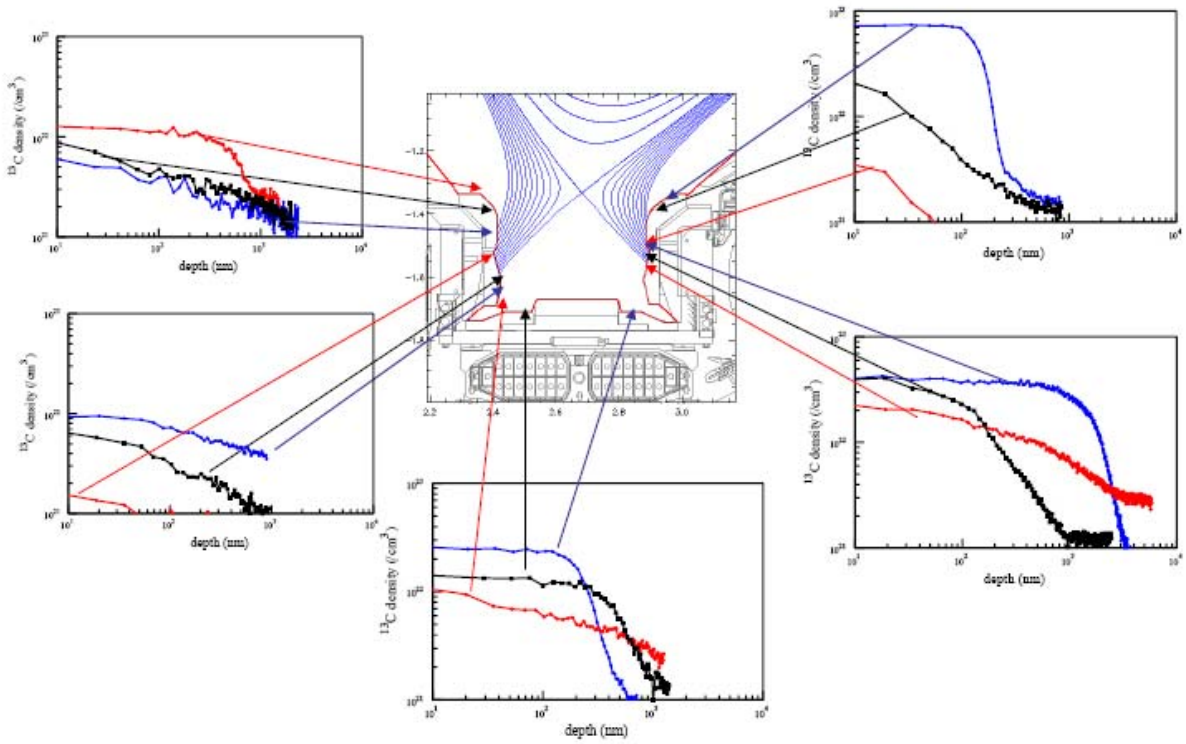

Figure 8

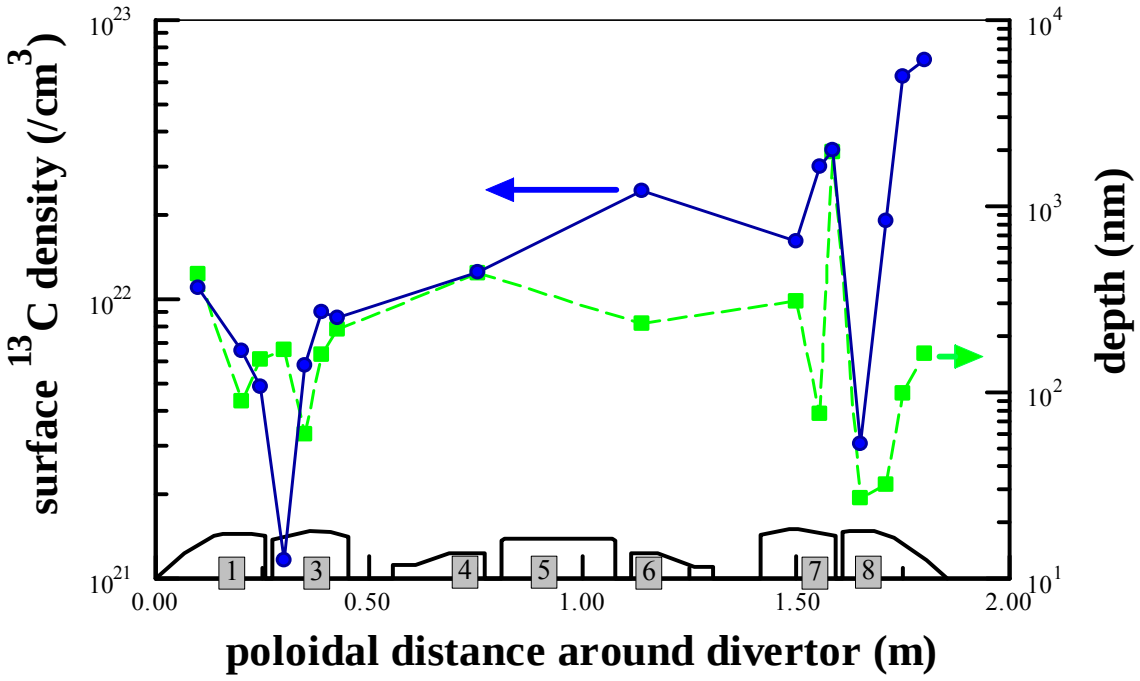
surface ^{13}C density (/cm^3)
depth (nm)
poloidal distance around divertor (m)
10^{23}
10^{22}
10^{21}
10^4
10^3
10^2
10^1
0.00
0.50
1.00
1.50
2.00
1
3
4
5
6
7
8

Figure 9

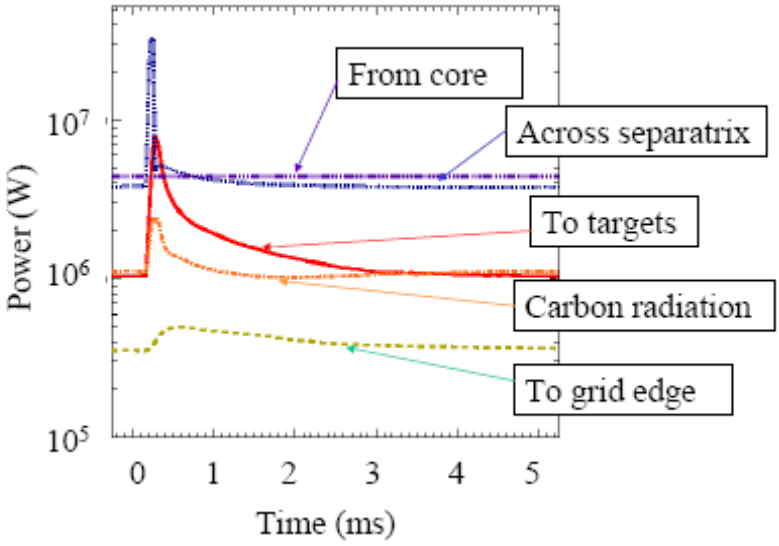
From core
Across separatrix
To targets
Carbon radiation
To grid edge
Power (W)
10^7
10^6
10^5
0
1
2
3
4
5
Time (ms)

Figure 10

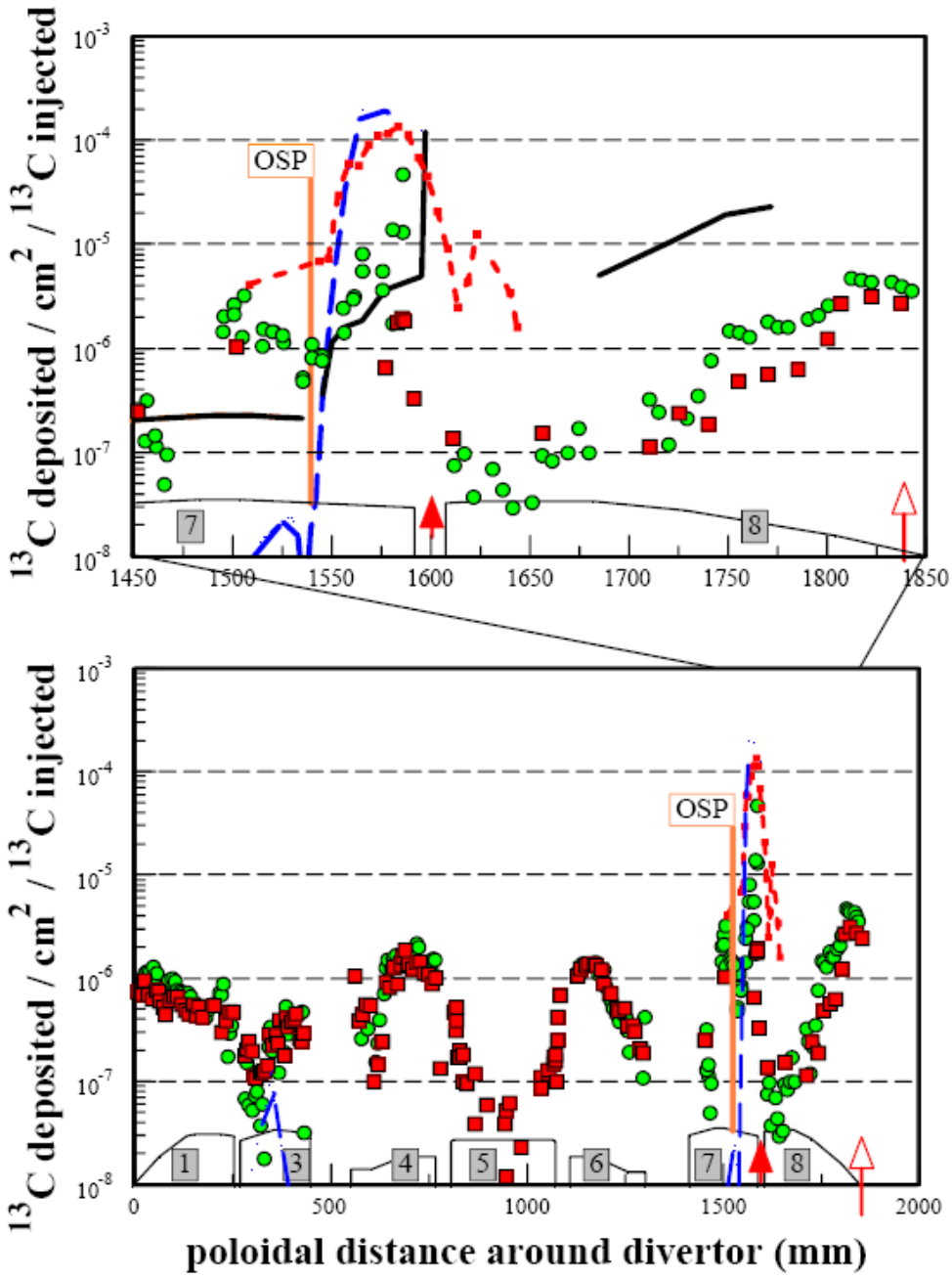
^{13}C deposited / cm^2 / ^{13}C injected
OSP
7
8
1450
1500
1550
1600
1650
1700
1750
1800
1850
^{13}C deposited / cm^2 / ^{13}C injected
OSP
1
3
4
5
6
7
8
0
500
1000
1500
2000
poloidal distance around divertor (mm)

Figure 11

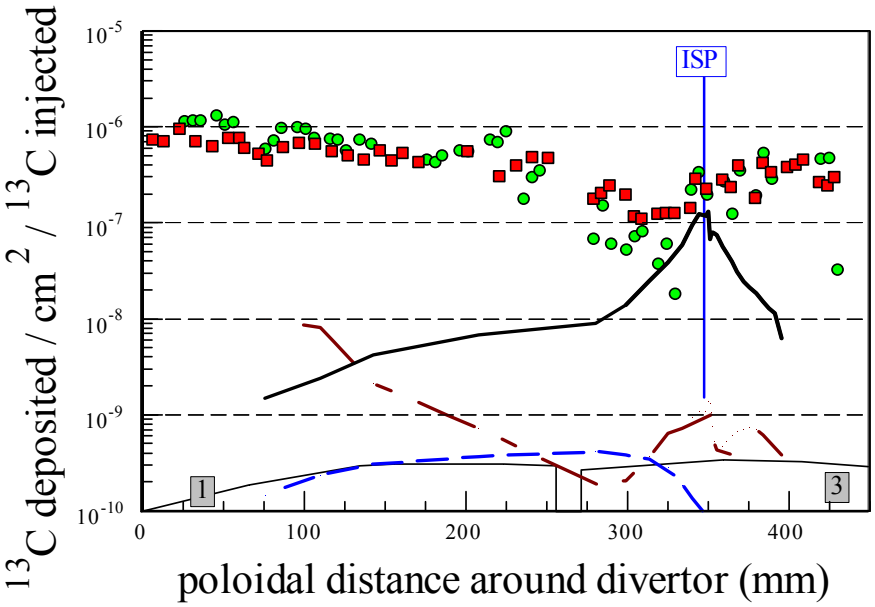
^{13}C deposited / cm^{2} / ^{13}C injected
10^{-5}
10^{-6}
10^{-7}
10^{-8}
10^{-9}
10^{-10}
ISP
1
3
0
100
200
300
400
poloidal distance around divertor (mm)

Figure 12

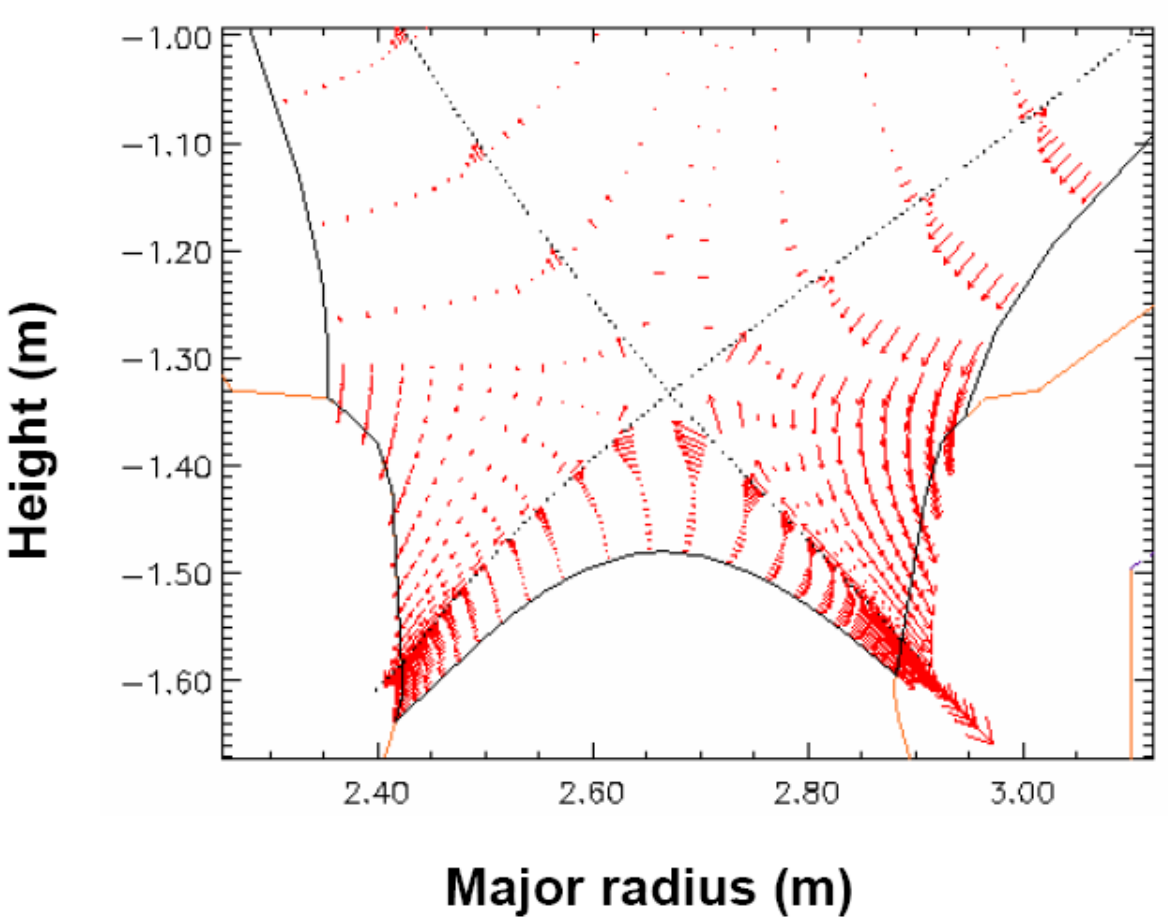
−1.00
−1.10
−1.20
−1.30
−1.40
−1.50
−1.60
Height (m)
2.40
2.60
2.80
3.00
Major radius (m)

Figure 13

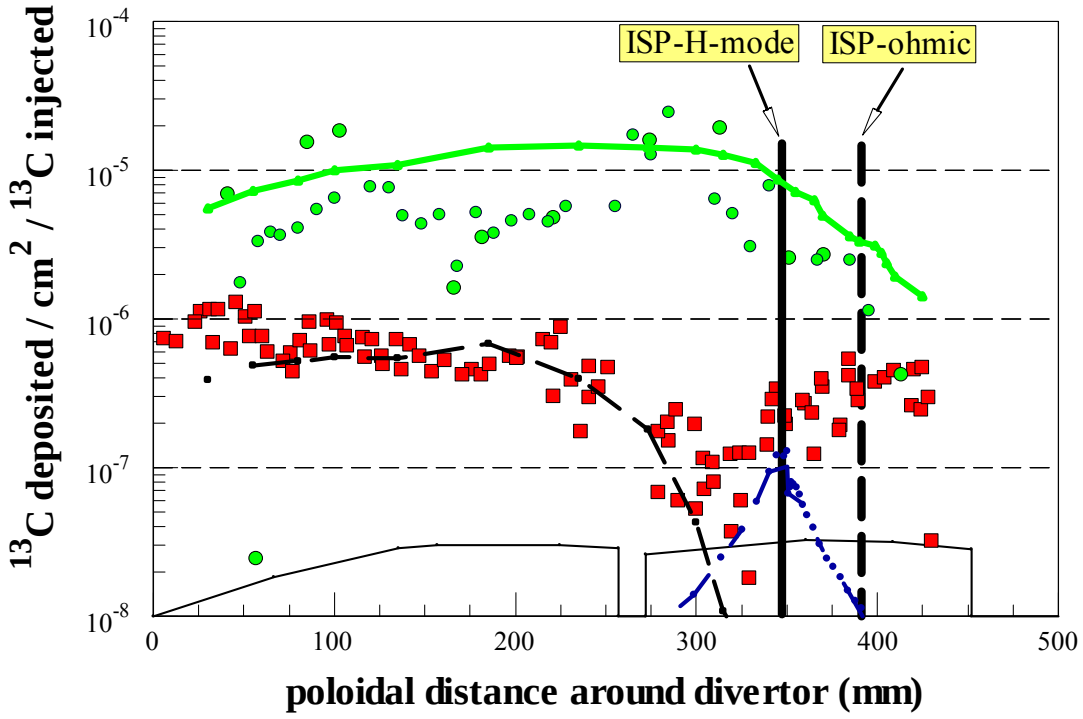
ISP-H-mode
ISP-ohmic
^{13}C deposited / cm^2 / ^{13}C injected
10^{-4}
10^{-5}
10^{-6}
10^{-7}
10^{-8}
0
100
200
300
400
500
poloidal distance around divertor (mm)

Figure 14

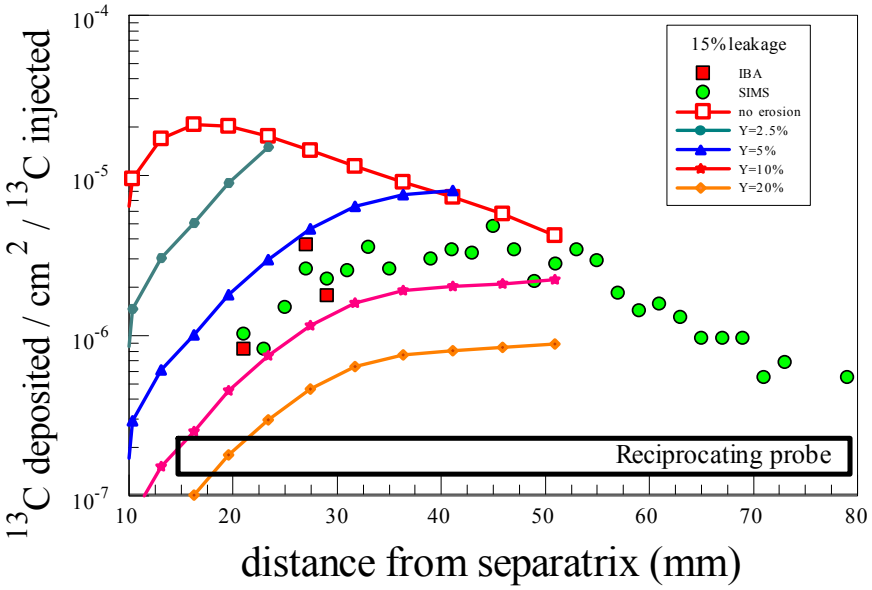
15% leakage
IBA
SIMS
no erosion
Y=2.5%
Y=5%
Y=10%
Y=20%
Reciprocating probe
^{13}C deposited / cm^{2} / ^{13}C injected
distance from separatrix (mm)
10^{-4}
10^{-5}
10^{-6}
10^{-7}
10
20
30
40
50
60
70
80

Figure 15

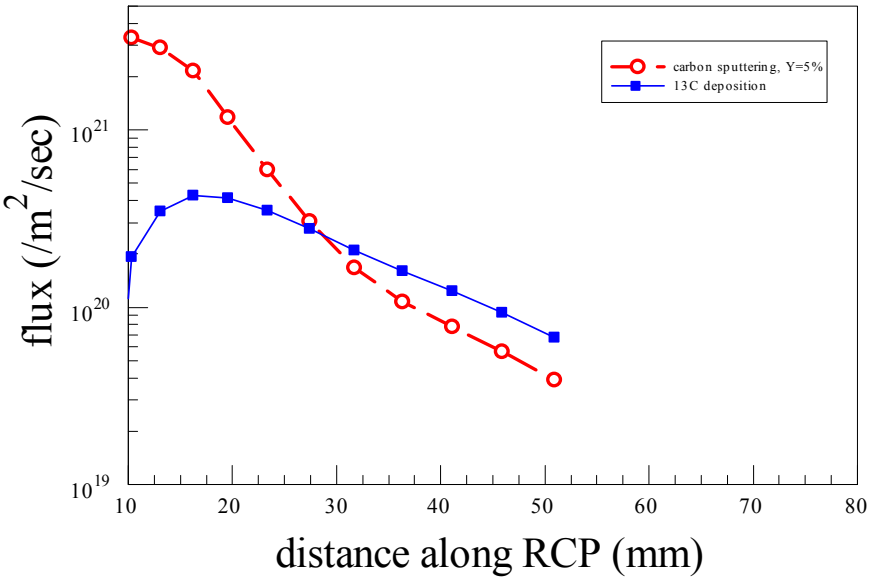
carbon sputtering, Y=5%
13C deposition
flux (/m2/sec)
10^21
10^20
10^19
10
20
30
40
50
60
70
80
distance along RCP (mm)

Figure 16

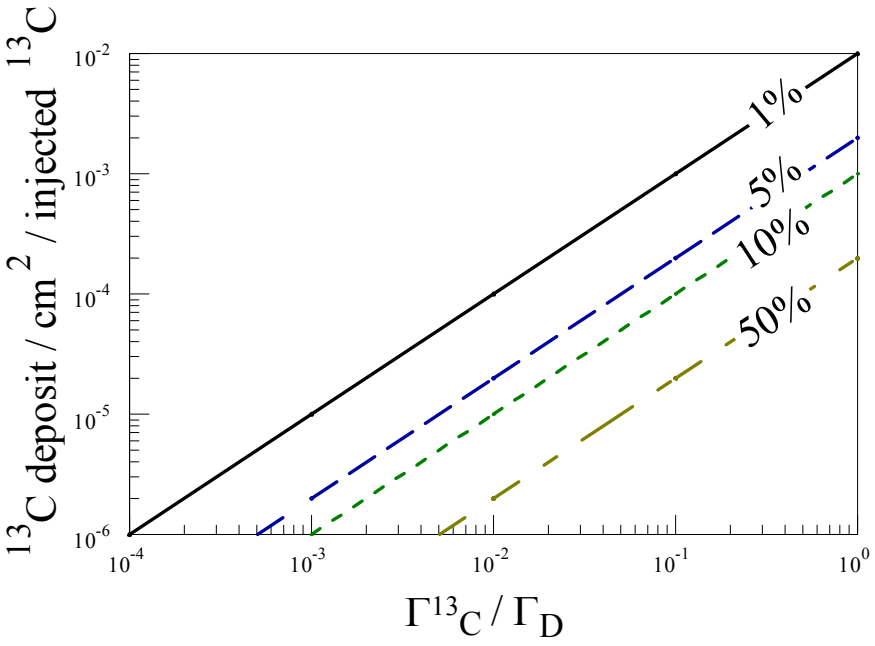
^{13}C deposit / cm^{2} / injected ^{13}C
10^{-2}
10^{-3}
10^{-4}
10^{-5}
10^{-6}
10^{-4}
10^{-3}
10^{-2}
10^{-1}
10^{0}
$\Gamma^{13}C / \Gamma_D$
1%
5%
10%
50%

Figure 17

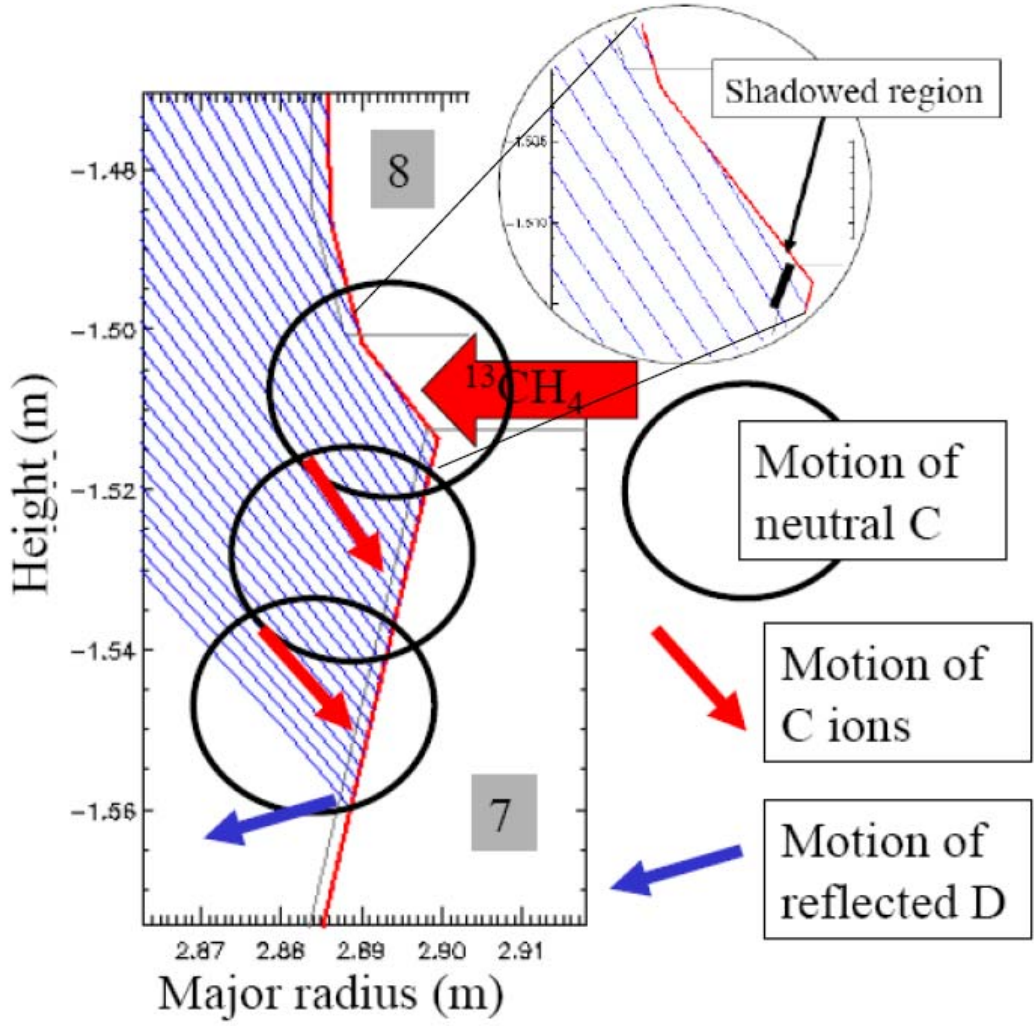
Shadowed region
8
7
$^{13}CH_4$
Motion of neutral C
Motion of C ions
Motion of reflected D
Height (m)
−1.48
−1.50
−1.52
−1.54
−1.56
2.87
2.88
2.89
2.90
2.91
Major radius (m)

Figure 18

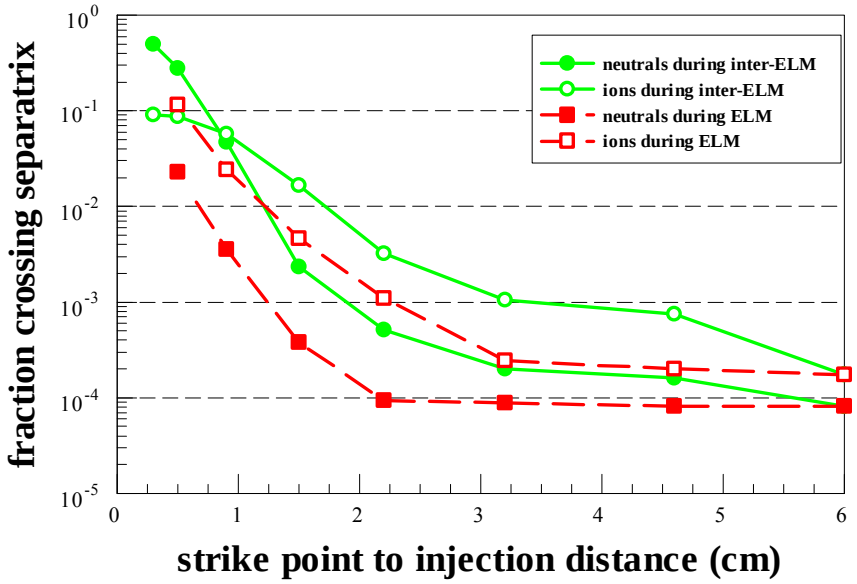
fraction crossing separatrix
strike point to injection distance (cm)
neutrals during inter-ELM
ions during inter-ELM
neutrals during ELM
ions during ELM
10^0
10^-1
10^-2
10^-3
10^-4
10^-5
0
1
2
3
4
5
6

Figure 19

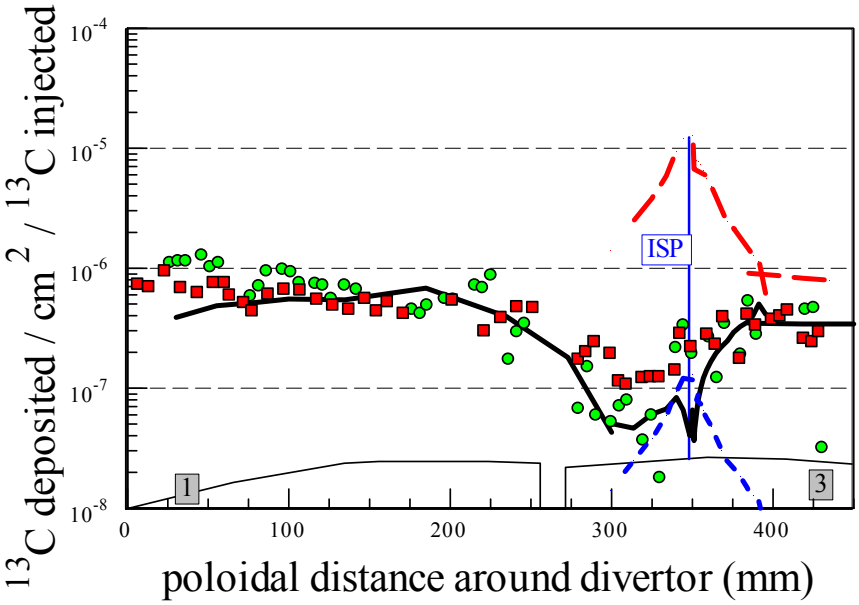
^{13}C deposited / cm^{2} / ^{13}C injected
10^{-4}
10^{-5}
10^{-6}
10^{-7}
10^{-8}
0
100
200
300
400
poloidal distance around divertor (mm)
ISP
1
3

Figure 20

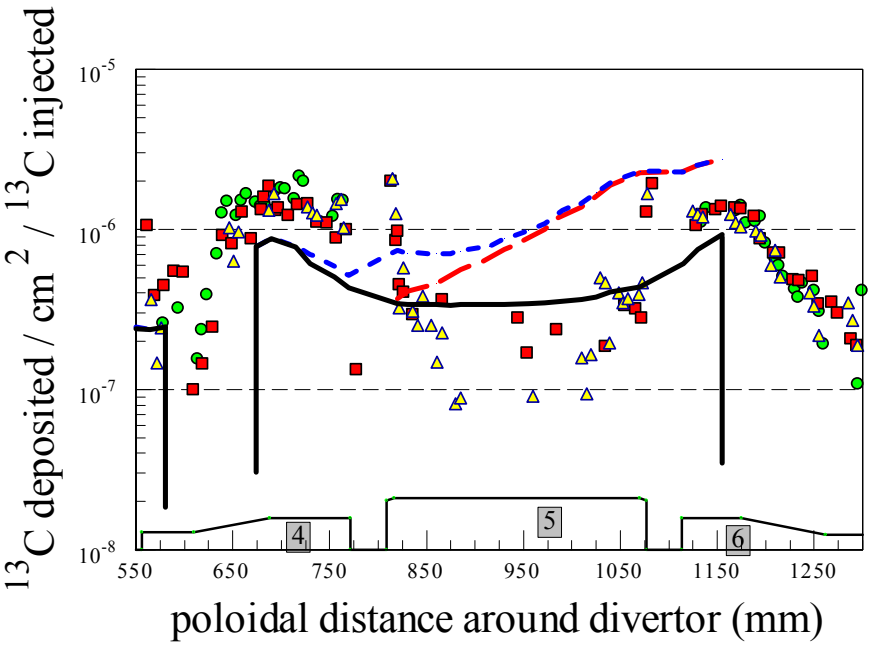
^{13}C deposited / cm^{2} / ^{13}C injected
10^{-5}
10^{-6}
10^{-7}
10^{-8}
550
650
750
850
950
1050
1150
1250
4
5
6
poloidal distance around divertor (mm)

Figure 21

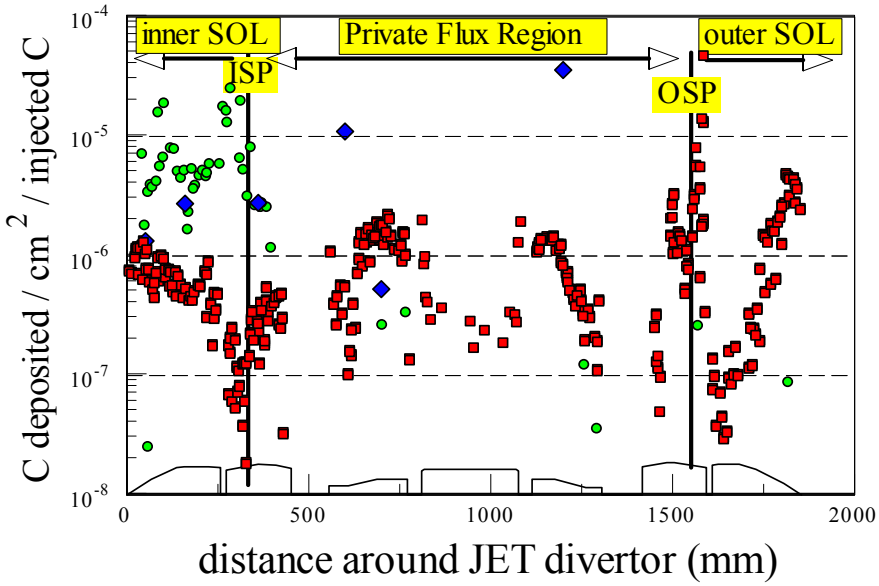
inner SOL
Private Flux Region
outer SOL
ISP
OSP
C deposited / cm 2 / injected C
10-4
10-5
10-6
10-7
10-8
0
500
1000
1500
2000
distance around JET divertor (mm)

Figure 22

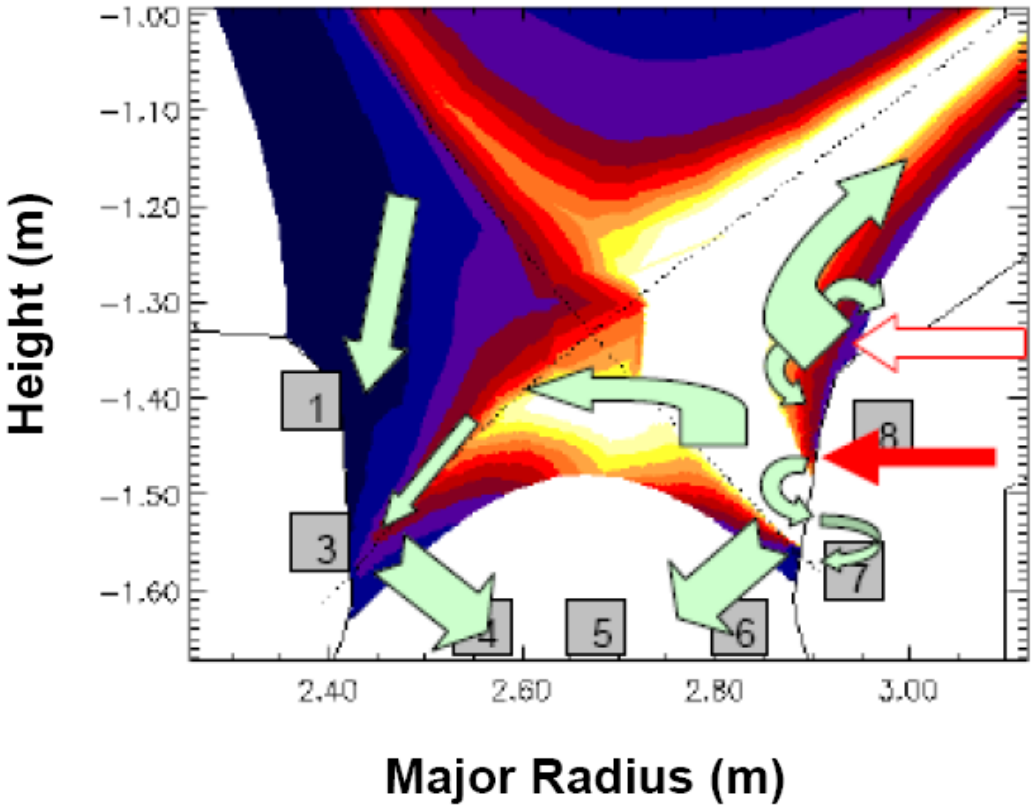
−1.00
−1.10
−1.20
−1.30
−1.40
−1.50
−1.60
Height (m)
1
3
4
5
6
7
8
2.40
2.60
2.80
3.00
Major Radius (m)

The Princeton Plasma Physics Laboratory is operated
by Princeton University under contract
with the U.S. Department of Energy.

Information Services
Princeton Plasma Physics Laboratory
P.O. Box 451
Princeton, NJ 08543

Phone: 609-243-2750
Fax: 609-243-2751
e-mail: pppl_info@pppl.gov
Internet Address: http://www.pppl.gov